This article has been accepted for publication in a future issue of this journal, but has not been fully edited. Content may change prior to final publication. Citation information: DOI 10.1109/JESTPE.2014.2331059, IEEE Journal of Emerging and Selected Topics in Power Electronics

Reduced-Order Electrochemical Model Parameters Identification and SOC Estimation for Healthy and Aged Li-Ion Batteries

Part I: Parameterization Model Development for Healthy Batteries

Ryan Ahmed, Mohammed El Sayed, Ienkaran Arasaratnam, Jimi Tjong, Saeid Habibi

***Abstract*— The current phase in our transportation system represents a paradigm shift from conventional, fossil-fuel-based vehicles into the second generation electric and hybrid vehicles. Electric vehicles provide numerous advantages compared to conventional vehicles since they are more efficient, sustainable, greener, and cleaner. The commercial market penetration and success of electric vehicles are tied to the efficiency, safety, cost, and lifetime of the traction battery pack. One of the current key electrification challenges is to accurately estimate the battery pack state of charge and state of health and therefore provide an estimate of the remaining driving range at various battery states of life. In order to estimate the battery state of charge, a high-fidelity battery model along with a robust, accurate estimation strategy are necessary. This paper provides three main contributions: (1) introducing a new state of charge parameterization strategy and utilizing it in setting up optimizer constraints to estimate battery parameters, (2) identification of the full-set of the reduced-order electrochemical battery model parameters using non-invasive genetic algorithm optimization on a fresh battery, (3) model validation using real-world driving cycles. Extensive tests have been conducted on Lithium Iron Phosphate-based cells widely utilized in high power automotive applications. Models can be effectively utilized onboard of battery management system.**

***Index Terms*— Battery parameters identification, electric vehicles, electrochemical battery model, genetic algorithm optimization, lithium-Ion batteries.**

I. INTRODUCTION

IN a series of two papers, the authors propose a complete solution for electrochemical battery modeling parameters identification and state of charge estimation at all battery states of life. The technique has been effectively applied to LiFePO4 cells and is applicable to any other battery chemistry. The papers cover battery mathematical modeling and parameterization, parameters identification, and state of charge estimation for fresh and aged batteries. This paper (Part I) investigates how to identify the full-set of the reduced-order electrochemical model parameters using genetic algorithm optimization. The paper includes a new parameterization strategy for state of charge calculation. In addition, a detailed illustration of the experimental setup and experiments conducted for data generation is presented. The paper also includes description of the electric vehicle model developed to generate the current profile from the velocity profile in addition to model fitting and validation. Part II of this paper presents the development of an aging and degradation model based on electrochemistry. The model accommodates for battery aging and provides an accurate estimate of the battery state of charge even at the battery end-of-life. The model works by changing the electrode effective volume along with tracking changes in the model parameters such as the diffusion coefficients and solid-electrolyte interface resistance. The model has been validated using real-world driving cycles for both fresh and aged battery cells. Furthermore, a state of charge and critical surface charge estimation strategy based on the reduced-order electrochemical model has been effectively applied. This section presents research motivation and technical challenges, summary of the recent literature, major paper contributions, and the paper outline.

Manuscript received December 1, 2013; revised January 30, 2014; accepted April 30, 2014. The review of this paper was co-ordinated by R. Ahmed.

R. Ahmed, M. El Sayed, I. Arasaratnam and S. Habibi are with the Department of Mechanical Engineering at McMaster University, Hamilton, ON, L8S4L7, Canada (e-mail:ryan.ahmed@mcmaster.ca; abugabma@mcmaster.ca, haran@ieee.org, habibi@mcmaster.ca).

J. Tjong is with Ford Motor Company of Canada, Windsor, ON N8Y 1W2 (jtjong@ford.com).

A. Motivation and Technical Challenges

Electric Vehicles (EVs) have received substantial attention in the last decade since they represent a sustainable transportation system compared to their petroleum-based counterparts. EVs provide a significant advantage due to the fact that electricity can be obtained from numerous energy sources such as nuclear, renewables (e.g.: solar, wind, and tidal), and fossil-fuels. Furthermore, EVs can recapture a portion of the energy lost during regenerative braking and can be restored in an on-board battery pack thus increases efficiency. EVs are more efficient compared to conventional gasoline vehicles since EVs have less moving mechanical parts and they do not require regular oil change [1]. Another main advantage is that EVs do not require replacement for the exhaust system since EVs do not produce emissions and do

not use conventional gearboxes [1].

Electric vehicles are usually driven by an on-board lithium-Ion battery pack which represents the core of the entire vehicle powertrain and requires precise monitoring and control. The battery management system (BMS) is responsible for real-time monitoring and control of various parameters such as state of charge (SOC), state of health (SOH), and remaining useful life (RUL). The main limitations of EVs penetration in the automotive market are: cost, range anxiety, safety concerns, and resale value (fear of battery degradation in performance). Regarding cost, the battery represents the most expensive component in the entire electric vehicle powertrain thus the price of an electric vehicle can be significantly reduced by economies of scale, for example, the cost of 1kWh is estimated to be approximately $1000 for a lithium-Ion battery cell and the objective is to bring it down to $250 within the coming couple of years [2]. Price can also be reduced by implementing an accurate SOC estimation strategy which would help to reduce the extra kWhs required due to battery overdesign. As for range anxiety, application of an accurate onboard SOC estimation strategies is of utmost importance; this will facilitate commercialization and wide-acceptance of electric vehicles which will eventually bring down the cost. Regarding safety and resale value concerns, these can be mitigated by incorporating a SOC estimation technique to avoid battery over charge and under discharge which significantly reduce the life time of the battery pack. Furthermore, accurate SOH estimation techniques and battery lifetime prediction (prognosis) approaches are necessary to assess battery degradation and provide the driver with information regarding the remaining useful life (RUL) which increases reliability and customer satisfaction.

In order to monitor the battery SOC and SOH, an accurate, high-fidelity battery mathematical model has to work collaboratively with an accurate and robust estimation strategy. For EV applications, battery SOC and SOH monitoring is an extremely challenging task; this is due to the fact that there are numerous parameters that interact together and affect battery performance. Batteries run under dynamic environment of acceleration and deceleration depending on the driving cycle, many factors affect the battery models and estimators accuracy such as imbalance between cells, self-discharge, aging effects, capacity fade, and temperature effects [3].

B. Literature Review

Electrochemical battery models (ECMs) have been widely researched in the recent literature since they are capable of modeling the diffusion of lithium inside the electrolyte and the electrodes. In contrast to equivalent circuit-based models and lumped-parameters models, ECMs represent a more attractive approach since they can provide an insight of the internal physical states and limitations of the battery, which is of extreme importance in automotive applications in which the battery is exposed to high transient current loads under various driving cycles [4].

Various attempts have been presented in the literature to estimate the electrochemical model parameters for both reduced and full-order models. In general, electrochemical battery model parameters such as diffusion coefficient and maximum solid lithium concentration are proprietary information, so they are commonly not provided by battery manufacturers. ECM parameters can be experimentally measured by examining the cells but this approach is costly, time consuming, and commonly not practical to obtain all parameters. Another approach, which is adopted in this paper, is to use non-destructive test using optimization techniques to fit models to experimental data.

In [4], experimental identification of the reduced-order electrochemical model parameters of a lithium-polymer cell is illustrated. Using continuous and pulse charging/discharging experimental data on a 6.8Ah, 9 model parameters are identified and the rest of the parameters are obtained from the literature [4]. Examples of the identified model parameters include: solid particle diffusion coefficients, electrode surface area, and maximum solid electrode potentials [4]. In [5], a genetic algorithm optimization technique has been applied to identify the parameters of the full-order electrochemical model using non-invasive experimental data from the input current and measured voltage [5]. Furthermore, fisher information technique has been applied to identify the accuracy of the resulting parameters [5]. The test has been conducted using liFePO4 cells from A123 [5]. The cells are used for high power applications which is the case in automotive traction battery pack [5].

C. Contributions

This paper presents a generic technique that can be used to estimate the electrochemical battery model parameters using non-invasive optimization strategy at any battery state of life. Based on the current literature and up to the authors' best knowledge, the full-set of the reduced-order electrochemical model parameters have not been identified using a real-world driving cycle while calculating the state of charge. Furthermore, no state of charge parameterization model has been developed to adjust the spherical volume-based state of charge calculation accordingly. Therefore, this paper overcome this gap in the literature and provides a generic technique for parameters identification using genetic algorithm. The technique has been used to estimate the full-set of the reduced-order electrochemical model parameters based on a 3.3V, 2.3Ah Lithium Iron Phosphate (LiFePO4) batteries at various states of life. Furthermore, the paper introduces a new electrochemical model-based SOC parameterization strategy based on the number of spherical shells (model states) and on the final value theorem. The final value theorem is applied in order to calculate the initial values of lithium concentrations at various shells of the electrode. Then, this value has been used in setting up a constraint for the optimizer in order to achieve accurate SOC estimation. Developed battery models at various battery states of life can be utilized in a real-time battery management system.

This article has been accepted for publication in a future issue of this journal, but has not been fully edited. Content may change prior to final publication. Citation information: DOI 10.1109/JESTPE.2014.2331059, IEEE Journal of Emerging and Selected Topics in Power Electronics

In order to fit ECM parameters, electric current input from an Urban Dynamometer Driving Schedule (UDDS) has been used. This current has been selected since it entails fast changing signal which is rich in its frequency content thus favored when optimization strategies are applied. Battery models have been validated using a variety of aggressive driving cycles such as the light duty drive cycle for high speed and high load (US06) and the highway fuel economy test (HWFET). In order to generate the current profile from driving cycle velocity profile, an electric vehicle model based on SimScape has been modified from an existing hybrid vehicle model and controller parameters have been tuned accordingly [6].

D. Paper Outline

The paper is organized as follows: section II describes the reduced-order electrochemical battery model. Section III illustrates the current generation process from the velocity profile and presents a summary of the experimental setup used. Section IV summarizes reference performance tests conducted on fresh and aged battery cells. Section V demonstrates the proposed model parameterization strategy and optimizer constraints. Section VI illustrates the parameter identification technique using genetic algorithm. Finally, section VII presents conclusions, limitations, and future work.

II. THE DOYLE-FULLER NEWMAN BATTERY MODEL

This section summarizes the reduced-order electrochemical battery model [7]. The reduced-order model is an approximation of the full-order Doyle-Fuller Newman Model [8]. Model reduction and discretization processes are illustrated in details to facilitate results replication for other researchers. Since this paper focuses on the reduced-order model, a brief summary of the Doyle-Fuller-Newman electrochemical model equations are presented in APPENDIX A and model details can be found in [8, 5]. A reduced-order form of the model is generally preferred in estimation and control applications, since full-order models are relatively computationally expensive which makes them difficult for online application in BMS [8].

A. The Reduced-Order Electrochemical Model

As shown in Fig. 1, a typical lithium-Ion battery comprises of two electrodes and a separator immersed in an electrolyte solution. The negative electrode (anode) is made of carbon and the positive electrode (cathode) consists of a metal oxide. Battery charging and discharging processes occur by transferring lithium ions between anode to the cathode across the solution and electrons through the current collectors [9]. The negative electrode half reaction is [8]:

$$Li_xC_6 \leftrightarrows C_6 + xLi^+ + xe^-$$

The half reaction for the positive electrode is as follows [8]:

$$Li_{y-x}Mn_2O_4 + xLi^+ + xe^- \leftrightarrows Li_yMn_2O_4$$

The overall battery reaction is described by the flowing equation [8]:

$$Li_{y-x}Mn_2O_4 + Li_xC_6 \leftrightarrows Li_yMn_2O_4 + C_6$$

The battery discharging reaction is represented by the right arrow direction and the charging process is presented by the left arrow [8]. Modeling the entire battery diffusion dynamics across both electrodes and the electrolyte, which is known as the Full-order model, is a computationally expensive task. Therefore, in order to implement the model onboard of a battery management system, model reduction has to be conducted. As shown in Fig. 1, a single particle is selected to represent each electrode and spherical diffusion inside this particular particle is considered.

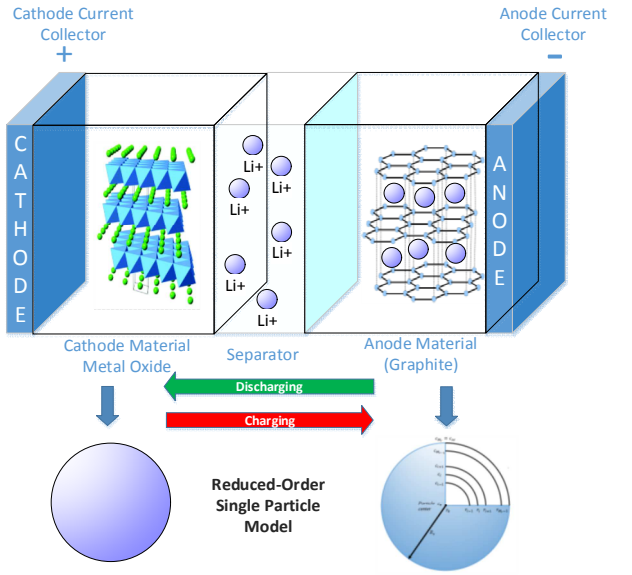

Fig. 1. Lithium-Ion Battery Structure and the Reduced-Order Model Assumption (Adopted from [8])

The reduced-order model used in this paper is known as the average model [8]. Several assumptions are carried out which results in a reduction in model accuracy. However, the model is still reliable to be applied for control and estimation purposes, such as state-of-charge and state-of-health estimation. The following assumptions have been made [8]:

- Each lithium-ion electrode is assumed to be a single sphere whose surface area is scaled to that of the porous electrode as shown in Fig. 1.
- Lithium concentration in the electrolyte and all model parameters are assumed to be held constant.
- No aging or capacity fade has been accounted for and all thermal effects are ignored.

Any of the above aforementioned approximations can be accounted for at the expense of an increased model complexity and computational requirements. The algorithm of the simplified averaged electrochemical model can be divided into 3 sub-models, namely: spherical diffusion sub-model, solid electrolyte interface concentration to terminal voltage sub-model, and solid concentration to SOC sub-model. These sub-models are discussed in details below:

Spherical diffusion sub-model

A single particle of radius R_s representing the entire

This article has been accepted for publication in a future issue of this journal, but has not been fully edited. Content may change prior to final publication. Citation information: DOI 10.1109/JESTPE.2014.2331059, IEEE Journal of Emerging and Selected Topics in Power Electronics

electrode is chosen as shown in Fig. 2. Accordingly, the spatial dimension x across the electrode is ignored. A summary of the model parameters are summarized in Table 1 [8]. The reduced-order model utilizes only one representative particle for each of the anode and the cathode. The sphere is divided into number of equal thickness shells.

TABLE 1.
ELECTROCHEMICAL BATTERY MODEL PARAMETERS NOMENCLATURE AND UNITS [8]

SYMBOL	NAME	UNIT
$\boldsymbol{i_e}$	Electrolyte current density	$A\ cm^{-2}$
$\boldsymbol{i_e}$	Solid current density	$A\ cm^{-2}$
$\boldsymbol{\emptyset_e}$	Electrolyte potential	V
$\boldsymbol{\emptyset_s}$	Solid potential	V
$\boldsymbol{c_e}$	Electrolyte concentration	$mol\ cm^{-3}$
$\boldsymbol{c_s}$	Solid concentration	$mol\ cm^{-3}$
$\boldsymbol{c_{se}}$	Concentration at the solid electrolyte interface	$mol\ cm^{-3}$
$\boldsymbol{J_{Li}}$	Butler-Volmer current	$A\ cm^{-3}$
$\boldsymbol{\theta_n}$	Anode Normalized solid concentration	-
$\boldsymbol{\theta_p}$	Cathode Normalized solid concentration	-
$\boldsymbol{U}$	Open circuit potential	V
$\boldsymbol{U_n}$	Anode open circuit voltage	V
$\boldsymbol{U_p}$	Cathode open circuit voltage	V
$\boldsymbol{\eta}$	Overpotential	V
$\boldsymbol{F}$	Faraday's constant	$C\ mol^{-1}$
$\boldsymbol{I}$	Applied battery cell current	A
$\boldsymbol{R}$	Universal Gas constant	$J\ K^{-1}\ mol^{-1}$
$\boldsymbol{T}$	Temperature	K

The single spherical particle is divided into $M_r - 1$ shells each of size Δr with $i = 1, \dots, M_r - 1$ and $r_i = i\Delta r$, where:

$$\Delta r = \frac{R_s}{M_r} \tag{1}$$

As shown in Fig. 2, the particle is divided into spherical shells and the outer shell (M_r) is exposed to the input current on the solid-electrolyte interface. The diffusion inside the particle is described using Fick's law of spherical diffusion as follows [9]:

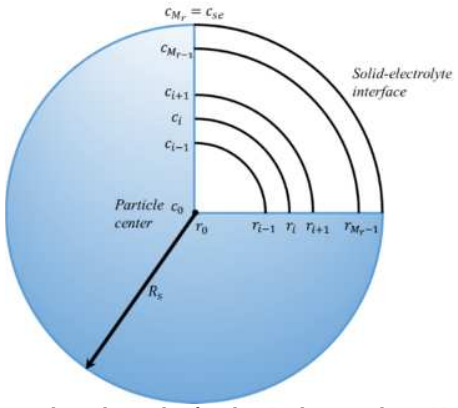

Fig. 2. Spherical Particle of Radius $\boldsymbol{R_s}$ discretized into $\boldsymbol{M_r}$ shells

$$\frac{\partial c_s}{\partial t} = \frac{\partial}{\partial r}\left(D_s \frac{\partial c_s}{\partial r}\right) \tag{2}$$

Where, c_s is the solid concentration at time t, and D_s is the diffusion coefficient. In order to discretize the aforementioned equation, consider the spherical particle as shown in Fig. 2 and that shell i is the shell of interest, in order to define the net flux diffusing from and into the shell, let's define the mole number N_2 from shell i to shell $i+1$ as [8]:

$$\delta N_2 = D_s \delta t A_i \left[c_{s_{i+1}} - c_{s_i}\right]/\delta r \tag{3}$$

Similarly, the mole number N_1 from shell $i-1$ to i can be expressed as follows:

$$\delta N_1 = D_s \delta t A_{i-1} \left[c_{s_i} - c_{s_{i-1}}\right]/\delta r \tag{4}$$

The net mole flux (per volume) into shell i can be written by subtracting (3) and (4) and dividing by the sphere volume V_i:

$$c_{s_i} = \frac{D_s \delta t}{\delta r}\left\{A_i\left[c_{s_{i+1}} - c_{s_i}\right] - A_{i-1}\left[c_{s_i} - c_{s_{i-1}}\right]\right\}/V_i \tag{5}$$

Substituting $A_i = 4\pi r_i^2$, $A_{i-1} = 4\pi r_{i-1}^2$, and $V_i = 4\pi\delta r\left[\frac{r_{i+1}+r_i}{2}\right]^2$ into (5) results in:

$$c_i = \frac{4D_s\delta t}{\delta r^2 (r_{i-1}+r_i)^2}\left\{r_i^2\left[c_{s_{i+1}} - c_{s_i}\right] - r_{i-1}^2\left[c_{s_i} - c_{s_{i-1}}\right]\right\} \tag{6}$$

By using the approximations $r_i^2 \cong r_{i-1}r_{i+1}$ and $(r_{i-1} + r_i)^2 \cong 4r_{i-1}r_i$ and substituting in (6) get [8]:

$$\delta c_{s_i} = \frac{D_s \delta t}{\delta r^2}\left\{c_{s_{i-1}} - 2c_{s_i} + c_{s_{i+1}} + (\delta r/r_i)\left(c_{s_{i+1}} - c_{s_{i-1}}\right)\right\} \tag{7}$$

Thus the rate of change of lithium concentration ($\delta c_{s_i}/\delta t$) in shell i can be described by the following equation:

$$\frac{\delta c_{s_i}}{\delta t} = \frac{D_s}{\delta r^2}\left\{c_{s_{i-1}} - 2c_{s_i} + c_{s_{i+1}} + (\delta r/r_i)\left(c_{s_{i+1}} - c_{s_{i-1}}\right)\right\} \tag{8}$$

Substituting $r_i = i\delta r$ into (8) and re-arranging terms gives:

$$\dot{c}_{s_i} = \frac{D_s}{\delta r^2}\left\{\left(\frac{i-1}{i}\right)c_{s_{i-1}} - 2c_{s_i} + \left(\frac{i+1}{i}\right)c_{s_{i+1}}\right\} \tag{9}$$

Equation (9) describes the rate of change of lithium concentration in any shell i, and can be used to specify the concentrations at various shells in addition to application of boundary conditions. By setting $i = 1, 2, .., M_{r-2}, M_{r-1}$ and defining $\alpha_1 = D_s/\delta r^2$ results in:

$$\dot{c}_1 = \alpha_1\left[-2c_{s_1} + 2c_{s_2}\right] \tag{10}$$

This article has been accepted for publication in a future issue of this journal, but has not been fully edited. Content may change prior to final publication. Citation information: DOI 10.1109/JESTPE.2014.2331059, IEEE Journal of Emerging and Selected Topics in Power Electronics

$$\dot{c}_{s_2} = \alpha_1 \left[\frac{1}{2} c_{s_1} - 2c_{s_2} + 3/2 c_{s_3}\right] \tag{11}$$

$$\dot{c}_{s_{M_r-2}} = \alpha_1 \left[\left(\frac{M_r-3}{M_r-2}\right) c_{s_{M_r-3}} - 2c_{s_{M_r-2}} + \left(\frac{M_r-1}{M_r-2}\right) c_{s_{M_r-1}}\right] \tag{12}$$

$$\dot{c}_{s_{M_r-1}} = \alpha_1 \left[\left(\frac{M_r-2}{M_r-1}\right) c_{s_{M_r-2}} - 2c_{s_{M_r-1}} + \left(\frac{M_r}{M_r-1}\right) c_{s_{M_r}}\right] \tag{13}$$

Two boundary conditions are set for the problem, one on the surface of the sphere as follows [8]:

$$D_s \frac{\partial c_s}{\partial r}\Big|_{r=R_s} = \frac{-J_{Li}}{a_s F}$$

And the other at the center of the sphere

$$D_s \frac{\partial c_s}{\partial r}\Big|_{r=0} = 0$$

The two boundary conditions at the sphere surface and the core, respectively can be re-written as follows:

$$D_s \left[(c_{s_{M_r}} - c_{s_{M_r-1}})/\delta r\right] = \frac{-J_{Li}}{a_s F} \tag{14}$$

$$D_s \left[(c_{s_1} - c_{s_0})/\delta r\right] = 0 \tag{15}$$

Re-arranging the previous equations results in [8]:

$$c_{s_{M_r}} = c_{s_{se}} = c_{s_{M_r-1}} - \delta r \frac{J_{Li}}{F a_s D_s} \tag{16}$$

$$c_{s_0} = c_{s_1} \tag{17}$$

Where $c_{s_{M_r}}$ is the solid concentration at the sphere outermost shell in contact with the electrolyte, and is thus referred to as solid electrolyte interface concentration (c_{se}). Substituting with the solid concentration at the core and at the surface in (10) and (13) and defining $\alpha_2 = 1/(F a_s \delta r)$ and re-arranging:

$$\dot{c}_{s_{M_r-1}} = \alpha_1 \left[\left(\frac{M_r-2}{M_r-1}\right) c_{s_{M_r-2}} - \left(\frac{M_r-2}{M_r-1}\right) c_{s_{M_r-1}} - \frac{\alpha_2}{\alpha_1}\left(\frac{M_r}{M_r-1}\right) J_{Li}\right] \tag{18}$$

Equations (10) to (12) along with (18) represent the single particle model and can be written in a state-space representation form as follows [8]:

System equation:

$$\dot{c}_s = A c_s + B u \tag{19}$$

Output equation:

$$c_{se} = c_{s_{M_r}} = c_{s_{M_r-1}} - \frac{\alpha_2}{\alpha_1} J_{Li} \tag{20}$$

Where, matrices *A* and *B* can be written as follows [8]:

$$A = \alpha_1 \begin{bmatrix} -2 & 2 & 0 & & & 0 & \\ 1/2 & -2 & 3/2 & \cdots & & 0 & \\ 0 & 2/3 & -2 & & & 0 & \\ & \vdots & & \ddots & & \vdots & \\ & & & & -2 & \frac{M_r-2}{M_r-3} & 0 \\ 0 & 0 & 0 & \cdots & \frac{M_r-3}{M_r-2} & -2 & \frac{M_r-1}{M_r-2} \\ & & & & 0 & \frac{M_r-2}{M_r-1} & \frac{2-M_r}{M_r-1} \end{bmatrix},$$

$$B = \alpha_2 \begin{bmatrix} 0 \\ 0 \\ \vdots \\ -\left(\frac{M_r}{M_r-1}\right) \end{bmatrix}$$

This sub-model has one input, one output, and M_{r-1} states representing the shells surface concentrations. The model input u is the butler-Volmer current (J^{Li}) which is a function of the solid electrolyte surface concentration (c_{se}) and the total current (I). The output of this sub-model is the solid concentration at the solid-electrolyte interface (c_{se}). This output is fed into another sub-model that calculates the terminal voltage.

Solid electrolyte interface-Terminal voltage sub-model:

Detailed description of the derivation of the following equations is discussed in [8]. Summary of the equations that uses the solid concentration at the solid-electrolyte interface to generate the terminal voltage are described in this subsection. The battery terminal voltage (from the full-order model) is calculated using equation (A18) in APPENDIX A and repeated here [8]:

$$V = \emptyset_s(x = L) - \emptyset_s(x = 0) - R_{SEI} I \tag{21}$$

The over-potential for the positive and negative electrodes η_p, and η_n is described by the following equations [8]:

$$\eta_p = \emptyset_{s,p} - \emptyset_{e.p} - U_p(c_{se,p}) \tag{22}$$

$$\eta_n = \emptyset_{s,n} - \emptyset_{e.n} - U_n(c_{se,n}) \tag{23}$$

This article has been accepted for publication in a future issue of this journal, but has not been fully edited. Content may change prior to final publication. Citation information: DOI 10.1109/JESTPE.2014.2331059, IEEE Journal of Emerging and Selected Topics in Power Electronics

Substituting (22) and (23) into (21) results in [8]:

$$V(t) = (\eta_p + \emptyset_{e.p} + U_p(c_{se,p})) - (\eta_n + \emptyset_{e.n} + U_n(c_{se,n})) \quad (24)$$

Grouping similar elements together results in [8]:

$$V(t) = (\bar{\eta}_p - \bar{\eta}_n) + (\bar{\emptyset}_{e.p} - \bar{\emptyset}_{e.n}) + \left(U_P(c_{se,p}) - U_n(c_{se,n})\right) - R_f I \quad (25)$$

The four terms in equation (25) are obtained separately as follows:

Open circuit Potential $\left(\boldsymbol{U_P(c_{se,p}) - U_n(c_{se,n})}\right)$**:**

The $c_{se,p}$ for the positive electrode is used to calculate the solid concentration at the solid-electrolyte interface for the negative electrode $c_{se,n}$ using the following equation [8]:

$$\bar{c}_{se,n} = c_{s,max,n}\left(\theta_{n0\%} + \frac{\bar{c}_{se,p} - \theta_{p0\%}c_{s,max,p}}{(\theta_{p100\%} - \theta_{p0\%})c_{s,max,p}}(\theta_{n100\%} - \theta_{n0\%})\right) \quad (26)$$

Where $\theta_{n0\%}$, $\theta_{n100\%}$, $\theta_{p0\%}$, $\theta_{p100\%}$ are the stoichiometry points for the negative and positive electrodes, respectively [10]. The solid concentrations at the electrode-electrolyte interface for the positive and negative particles are normalized as follows [8]:

$$\theta_p = \frac{solid - electrolyte\ concentration\ (positive\ )}{maximum\ solid\ concentration} = \frac{c_{se,p}}{c_{s,max,p}} \quad (27)$$

$$\theta_n = \frac{solid - electrolyte\ concentration\ (negative)}{maximum\ solid\ concentration} = \frac{c_{se,n}}{c_{s,max,n}} \quad (28)$$

Normalized concentration values in (27) and (28) range from 0 to 1 and are further used to obtain the open circuit potential equations for the cathode (Up) and for the anode (U_n). The experimental derivation of U_p and U_n is described in details in section IV.

The Overpotential $\left(\boldsymbol{\bar{\eta}_p - \bar{\eta}_n}\right)$

The difference between the anode and cathode overpotentials can be calculated using the following equations (details of the equations derivations can be found in [8]):

$$\bar{\eta}_n = \frac{RT}{\alpha_a F}\ln(\xi_n + \sqrt{\xi_n^2 + 1}) \quad (29)$$

$$\bar{\eta}_p = \frac{RT}{\alpha_a F}\ln(\xi_p + \sqrt{\xi_p^2 + 1}) \quad (30)$$

where,

$$\xi_n = \frac{\bar{j}_n^{Li}}{2a_s j_o} \quad (31)$$

$$\xi_p = \frac{\bar{j}_p^{Li}}{2a_s j_o} \quad (32)$$

Where, $\bar{j}_n^{Li}$ and $\bar{j}_n^{Li}$ are the Butler-Volmer currents defined as follows:

$$\bar{j}_n^{Li} = \frac{I}{A\delta_n} = a_s j_o[exp\left(\frac{\propto_a F}{RT}\bar{\eta}_n\right) - exp(\frac{\propto_c F}{RT}\bar{\eta}_n)] \quad (33)$$

$$\bar{j}_p^{Li} = \frac{I}{A\delta_p} = a_s j_o[exp\left(\frac{\propto_a F}{RT}\bar{\eta}_p\right) - exp(\frac{\propto_c F}{RT}\bar{\eta}_p)] \quad (34)$$

j_o can be calculated as follows:

$$j_o = (c_e)^{\alpha_a}(c_{s,max} - c_{se})^{\alpha_a}(c_{se})^{\alpha_c} \quad (35)$$

The electrolyte potential $\boldsymbol{(\bar{\emptyset}_{e.p} - \bar{\emptyset}_{e.n})}$

An approximate of the difference can be calculated using the following equation:

$$(\bar{\emptyset}_{e.p} - \bar{\emptyset}_{e.n}) = -\frac{I}{2A}(\frac{\delta_n}{k^{eff}} + \frac{\delta_n}{k^{eff}} + \frac{\delta_n}{k^{eff}}) \quad (36)$$

Solid Particle Concentration - SOC sub-model

The critical surface charge (CSC) for the positive electrode is calculated from the solid-electrolyte interface ($c_{se,p}$). Normalized solid-electrolyte concentration θ is obtained first using equation (27); the critical surface charge is calculated based on the positive electrode lithium concentration only using the following equation [8]:

$$CSC = \frac{\theta_p - \theta_{p0\%}}{\theta_{p100\%} - \theta_{p0\%}} \quad (37)$$

The battery state of charge (SOC) is calculated based on the spherical average concentration ($c_{s,p_{avg}}$) inside the positive electrode. The SOC is calculated as [8]:

$$\theta_{p_{avg}} = \frac{average\ positive\ sphere\ concentration}{maximum\ solid\ concentration} = \frac{c_{s,p_{avg}}}{c_{s,max,p}} \quad (38)$$

Where, the average solid particle concentration for the positive electrode ($c_{s,p_{avg}}$) is calculated by integrating the concentrations of electrode shells and dividing by the sphere volume as [8]:

This article has been accepted for publication in a future issue of this journal, but has not been fully edited. Content may change prior to final publication. Citation information: DOI 10.1109/JESTPE.2014.2331059, IEEE Journal of Emerging and Selected Topics in Power Electronics

$$c_{s,p_{avg}} = \frac{c_T}{V} = \frac{total\ lithium\ concetration}{particle\ volume} = \frac{\sum_{i=1}^{M_r-1} r_i^2 4\pi\Delta r}{\frac{4}{3}\pi(R_s - \Delta r)^3} \quad (39)$$

Then the SOC is calculated as [8]:

$$SOC = 100 * (\frac{\theta_{p_{avg}} - \theta_{p0\%}}{\theta_{p100\%} - \theta_{p0\%}}) \quad (40)$$

Note that the critical surface charge (i.e.: the charge at the solid-electrolyte interface) is not used in the calculation of the total battery state of charge. Alternatively, the solid electrolyte interface concentration is used for terminal voltage calculation. This explains the fact that when a zero current is applied to the battery, battery voltage exhibits relaxation effect, since lithium ions on the outer surface diffuse to lower concentration shells inside the particle thus voltage decreases until lithium concentration in all shells are equalized and no further diffusion takes place. On the other hand, the battery state of charge does not change upon applying a zero current input. Since the same lithium concentration is contained inside the sphere and averaged to obtain the overall battery SOC.

III. Current Generation and Experimental Setup

This section summarizes the process of current generation from the velocity profiles of various driving cycles. Then a summary of the experimental setup including cyclers, environmental chambers, data acquisition systems, and battery cells is provided.

A. Current generation

In order to generate the current profiles needed for experimentation, an electric vehicle battery model has been modified from an existing hybrid vehicle model [6]. The model has been simulated using SimScape in Matlab environment in order to obtain the current profile from the velocity profile. A mid-size vehicle sedan parameters have been used in the model with an approximate driving range of 200 kilometers per full charge. The simulation model, as shown in Fig. 3, consists of a vehicle dynamics model, DC electric motor, DC-DC convertor, lithium-Ion battery pack, and vehicle speed controller.

Three benchmark driving schedules have been used in the simulation; namely, an Urban Dynamometer Driving Schedule (UDDS), a light duty drive cycle for high speed and high load (US06), and a High fuel Economy Test (HWFET) [11]. Even though the driving behavior of an average driver may likely to vary, these driving cycles have been widely used in both industrial and academic settings to simulate various driving patterns.

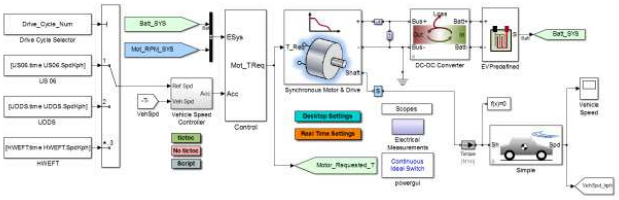

Fig. 3. All-Electric Mid-size Sedan Simulation Model in SimScape (Adopted from [6])

TABLE 2.
CHARACTERISTICS OF UDDS, US06, AND HWFET DRIVING SCHEDULES [11]

	LENGTH	DISTANCE	AVG SPEED (MPH)
UDDS	1,369	7.45	19.59
US06	596	8.01	48.37
HWFET	765	10.26	48.30

The UDDS driving cycle represents a city driving condition, the UDDS cycle (commonly known as “LA4” or “the city test” or Federal Test Procedure “FTP-72”) was originally used for light duty fossil-fueled vehicle testing [11]. It has been developed to imitate average speed, idle time, and number of stops that the average driver performs in practice [12].

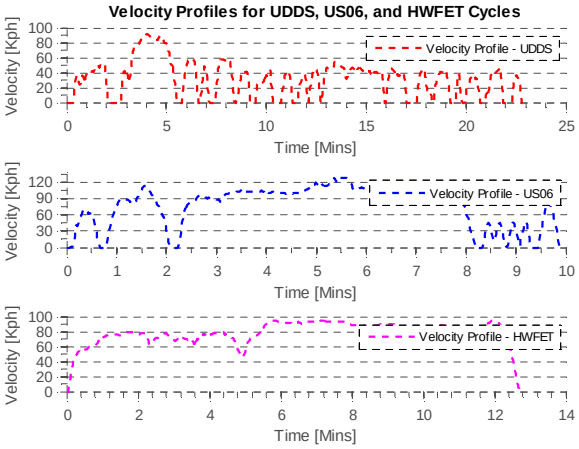

Fig. 4. Velocity Profiles for the UDDS (upper figure), US06 (middle), and HWFET (lower) Cycles [11]

The test profile is recommended by the U.S. Environmental Protection Agency to estimate the fuel economy in city driving conditions [11]. For electric vehicles, the profile has been extensively used to estimate the driving range in miles per full charge [13, 14]. The US06 cycle is a high acceleration, aggressive driving cycle, and the HWFET represents a highway driving conditions with speed below 60 miles/hour [15]. The three aforementioned driving cycles are as shown in Fig. 4 below. An exclusive summary of these driving cycle characteristics such as distance, time, and average speeds is as shown in Table 2 [16].

The pack current profiles from these driving cycles are as shown in Fig. 5. Since the US06 driving cycle is an aggressive driving cycle, the current demand by the motor is quite high compared to current profiles from the HWFET and the UDDS cycles. Current profiles have been scaled down to the cell

This article has been accepted for publication in a future issue of this journal, but has not been fully edited. Content may change prior to final publication. Citation information: DOI 10.1109/JESTPE.2014.2331059, IEEE Journal of Emerging and Selected Topics in Power Electronics

level and used for model parameters fitting.

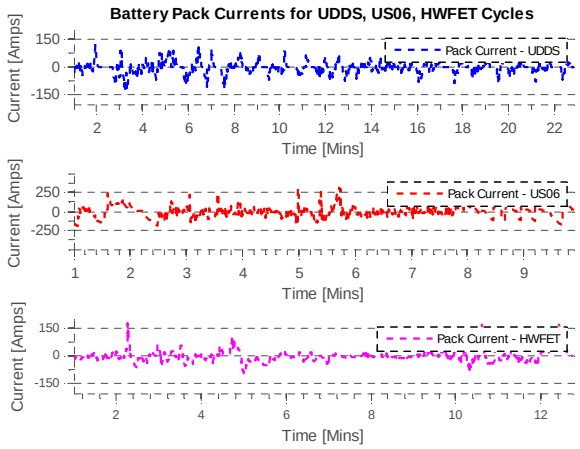

Fig. 5. Pack Current Profiles for the UDDS (Upper figure), US06 (middle figure), and HWFET (lower figure) Cycles

B. *Experimental Setup*

The experimental setup is as shown in Fig. 6, the setup includes 3 channel Arbin BT2000 tester, 3 lithium Iron Phosphate cells, 3 environmental chambers, AVL Lynx data acquisition system, and AVL Lynx user-interface software. AVL Lynx software is used for setting up the test procedure and for data acquisition.

Fig. 6. Experimental Setup including Cyclers, Environmental Chambers, and Data Acquisition Systems

Various variables such as battery current, voltage, and temperatures during charging, discharging, and rest phases are acquired at a maximum frequency of 50 Hz.

Battery test cells are placed in environmental chambers in order perform the test at controlled temperature conditions. Two different environmental chambers provided by two different companies are used for testing namely, Thermotron and Espec. These units can change the temperature from -70 to 180 ℃ and are able to change the temperatures at a rate of 3.5 $℃/min$. This kind of heating and cooling capability is necessary for stressing samples and accelerating battery aging and therefore saving total test time. Each battery is independently tested using separate tester channel.

Fig. 7. Arbin BT2000 Cycler along with Espec and Thermotron Environmental Chambers

The Arbin tester, as shown in Fig. 7 and Fig. 8, has 3 independent channels. The cycler can operate in two voltage operations ranges namely, High operation voltage: 0-5 V and low operation voltage: 0-20 V and 3 different current ranges: High operation range: 0 - ±400 Amps, Medium operation range: 0 - ±40 Amps, and Low operation range: 0 - ±5 Amps.

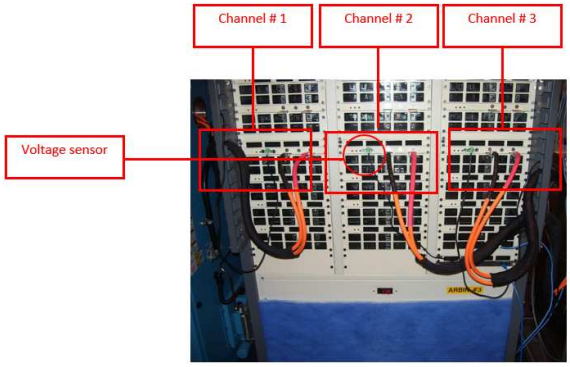

Fig. 8. Arbin Cycler channels: channels equipped with voltage sensor and status indicator light

This article has been accepted for publication in a future issue of this journal, but has not been fully edited. Content may change prior to final publication. Citation information: DOI 10.1109/JESTPE.2014.2331059, IEEE Journal of Emerging and Selected Topics in Power Electronics

IV. Reference Performance Tests and Experimental Data Analysis

A summary of the reference performance tests (RPT) conducted on fresh battery cells is presented in subsection *A*. In subsection *B*, an illustration of the data analysis conducted to generate the cathode and anode equilibrium potentials (U_p and U_n) is illustrated.

A. Characterization/RPT tests

Extensive characterization tests have been conducted on a fresh and aged batteries at controlled room temperature of 25℃, 4 main experiments include: A static capacity test at 1C rate, SOC-OCV characterization test, pulse charge/Discharge test, and Driving Cycle tests (e.g.: Urban Dynamometer Driving schedule) test. Characterization tests are conducted to specify battery cells baseline performance characteristics such as cell power capability, internal resistance, capacity, and time constants. The following tests are selected for the study:

Static Capacity Test – PNGV, 2001

This test is used to measure the battery cell capacity in Ampere-hours at a constant current (CC) discharge rate. This test is conducted in order to provide a baseline for a fresh battery cell capacity. The test procedure follows the constant current constant voltage (CCCV) protocol and is summarized in the following steps [17]:

1. *Charge the battery at 1C rate (2.3 A) to fully charged state in a constant current constant voltage (CCCV) mode. The battery is fully charged at 3.6 V and when the current end point is at 0.02 C (0.046 A).*
2. *Leave the battery to rest for one hour in order to allow for voltage and current stabilization* [17].
3. *Discharge sequence at a constant current 1C rate until the voltage reaches the battery minimum voltage limit (2 V) recommended by the manufacturer* [17].
4. *Battery is left at rest with no load for one hour.*

OCV-SOC Relationship:

This test is used to characterize the open-circuit voltage (OCV) - state of charge (SOC) relationship. Very small C-rates (C/20, C/15) are used for OCV-SOC characterization in order to minimize cell dynamics and to minimize ohmic loss effects due to battery internal resistances [18]. Accordingly, by conducting this experiment, the measured terminal voltage is assumed to be the open circuit voltage. This test is important since the cathode and anode electrode potentials (U_p and U_n), which are used in the electrochemical model, are being derived from this test as discussed in subsection *C*. The OCV-SOC relationship is obtained as follows (this test is similar to the capacity test but is conducted at a very low C-rate):

1. *Fully charge the battery in a CCCV mode until maxi mum voltage (3.6V).*
2. *Fully discharge the battery at constant current (CC) mode with 1C-rate until the voltage hits the minimum voltage (2V).*
3. *All cycler current accumulators are reset to zero. At this moment, the battery is at zero state of charge (SOC).*
4. *Charge the battery at a very small C-rate of C/15 (0.06*2.3=0.15A) in a CCCV mode until it hits the maximum voltage of 3.6V. The cell is left to rest for one hour to relax.*
5. *Discharge the cell at the same rate of C/15 until and the battery hits the minimum voltage of 2 V.*

The charging and discharging curves are averaged to obtain a single fixed relationship between OCV and SOC.

Driving cycles

Current profiles generated from the electric vehicle model as illustrated in section III are used to excite the cells. The pack current profile is scaled down to the cell level and is fed to the cycler. These driving cycles are very rich in their frequency content, since they include fast variations and will be used for model parameters fitting. The cell current is generated from the pack current by assuming no cell balancing (i.e.: all cells are held at the same state of charge) and by assuming equal current distributions among parallel cell branches.

B. Fresh Battery - Cathode/Anode Electrode Potential Derivation

The separate cathode and anode electrodes potential can be estimated from the SOC-OCV relationship. The OCV vs. time for both charging and discharging of a fresh battery is as shown in Fig. 9. The test has been conducted at C/15 rate. In order to obtain the OCV-SOC relationship, the OCV curves for both charging and discharging are plotted vs. SOC as shown in Fig. 10.

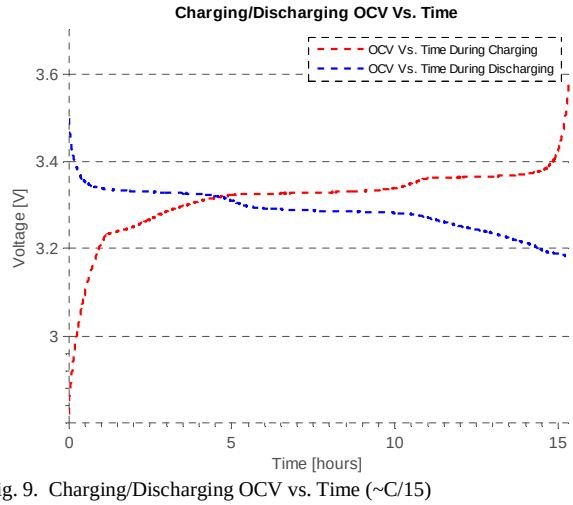

Fig. 9. Charging/Discharging OCV vs. Time (~C/15)

This relationship, as previously mentioned, is obtained by Cycling the battery at a very low C-rate (C/20 or C/15) to minimize battery dynamics and use the measured terminal voltage as the open circuit voltage (i.e.: assuming negligible

This article has been accepted for publication in a future issue of this journal, but has not been fully edited. Content may change prior to final publication. Citation information: DOI 10.1109/JESTPE.2014.2331059, IEEE Journal of Emerging and Selected Topics in Power Electronics

voltage drop on the internal resistance due to very low current) [18].

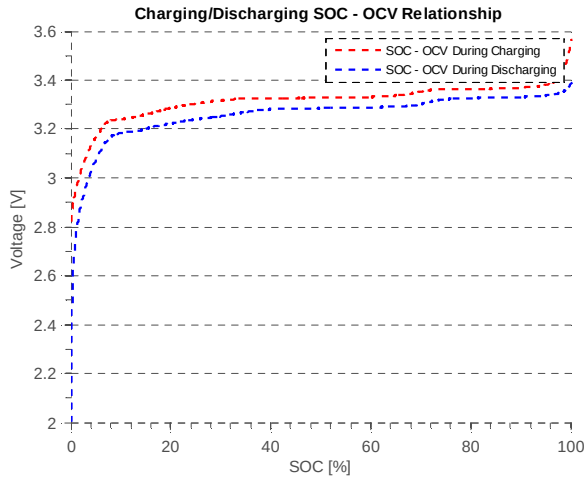

Fig. 10. SOC-OCV relationship for both charging and discharging

It is clear that the battery behavior during charging and discharging are not identical due to hysteresis effects which is obtained by subtracting both curves is shown in Fig. 11.

In order to obtain one curve to represent the OCV-SOC relationship, data has been resampled to 50 points for each of the charging/discharging curves then they have been averaged as shown in Fig. 12.

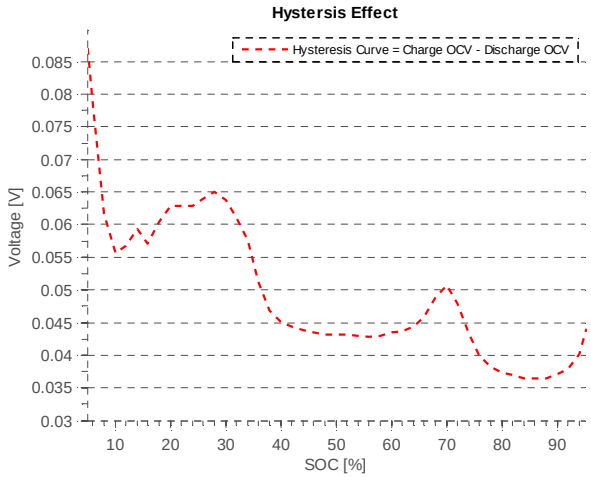

Fig. 11. Hysteresis Effect - Obtained by subtracting Charging and Discharging Curves

In order to obtain the open circuit potential for the positive electrode (U_p) and the negative electrode (U_n) from the OCV-SOC relationship shown in Fig. 12, one of the two electrode potential has to be independently calculated and then subtracted from the OCV-SOC relationship to derive the other. In this paper, since the negative electrode active material is made of graphite (Li_xC_6), the empirical relationship below [19] can be derived from the literature [20]. The anode electrode potential (U_n) as function of the normalized lithium concentration is as shown in Fig. 13 [5]. The empirical relationship is as follows [19]:

$$U_n(x) = C_1 + C_2x + C_3x^{1/2} - C_4x^{-1} + C_5x^{\frac{3}{2}} + C_6\exp[\,15(0.06 - x)] - C_7\exp[C_8(x - 0.92)]$$

Where, x is defined as the lithium concentration in the solid active material divided by the maximum permissible solid concentration [19]. The constants C_1 to C_8 values are as follows:

$$C_1 = 8.002296379,\ C_2 = 5.064722977,\ C_3 = -12.57808059,\ C_4 = 8.632208755e-4,\ C_5 = 2.179498281e-5,\ C_6 = -0.4601573522,\ C_7 = 0.5536351675,\ C_8 = -2.432630003$$

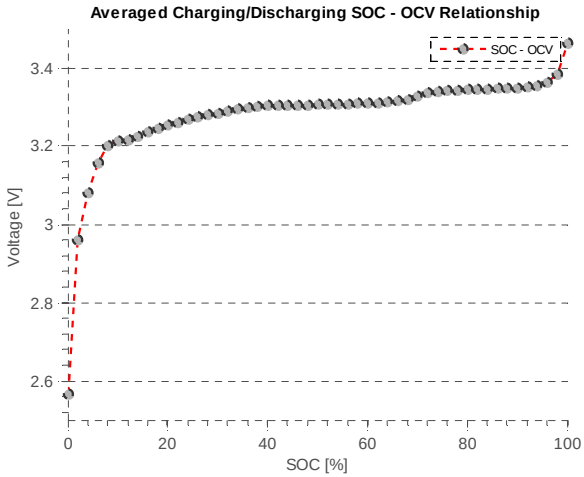

Fig. 12. Charging and Discharging Averaged SOC-OCV Curve

The cathode potential (U_p) is obtained from the anode potential by subtracting U_n from the OCV-SOC curve as shown in Fig. 14 below [5]. In each electrode, curves have been discretized to 50 control points and a Piecewise Cubic Hermite Interpolating Polynomial (PCHIP) is used perform interpolation between control points [5].

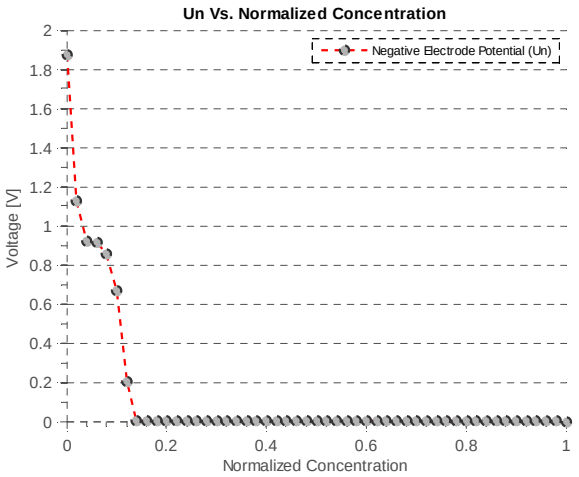

Fig. 13. Anode Equilibrium Potential Vs. Normalized Concentration [5]

This article has been accepted for publication in a future issue of this journal, but has not been fully edited. Content may change prior to final publication. Citation information: DOI 10.1109/JESTPE.2014.2331059, IEEE Journal of Emerging and Selected Topics in Power Electronics

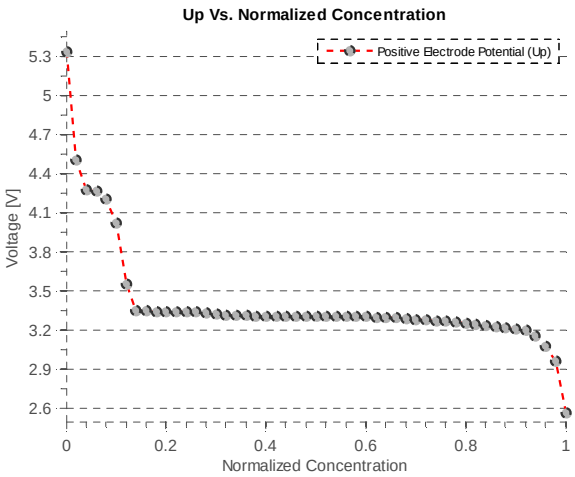

Fig. 14. Cathode Equilibrium Potential as function of Normalized concentration

V. Parameterization Model Development

In order to optimize the electrochemical battery model parameters, an objective function has to be set in order to fit the model output voltage to experimental data. In order to optimize the battery voltage while maintaining an accurate SOC estimate, model parameterization has to be conducted in order to scale the input current to the Butler-Volmer current values. This value is further applied as an input to the spherical particle for each electrode. This section provides a new parameterization model which is a function of the number of spherical shells (M_r). The model is further used as a constraint during parameters optimization. The following subsections illustrate the parameterization procedure by considering the reversed process of obtaining the initial lithium concentration from the initial SOC followed by deriving the parameterization equation.

A. Total sphere concentration from initial SOC

In order to start simulating the model, the initial lithium concentration values has to be calculated from the initial SOC. First, assuming a known battery SOC, an inverse SOC calculation has to be conducted as follows: Recall that the battery SOC is calculated based on the spherical average concentration ($c_{s,p_{avg}}$) inside the positive electrode (equations 39-40). Equations are repeated here for readability, the SOC is calculated as follows [8]:

$$SOC = 100 * \left(\frac{\frac{c_{s,p_{avg}}}{c_{s,max,p}} - \theta_{p0\%}}{\theta_{p100\%} - \theta_{p0\%}}\right)$$

Where, the average solid particle concentration for the positive electrode ($c_{s,p_{avg}}$) is calculated by integrating the concentrations of electrode shells and dividing by the sphere volume as follows [8]:

$$c_{s,p_{avg}} = \frac{c_T}{V} = \frac{total\ lithium\ concetration}{particle\ volume} = \frac{\sum_{i=1}^{M_r-1} r_i^2 4\pi\Delta r c_i}{\frac{4}{3}\pi(R_s - \Delta r)^3}$$

Thus assuming a known initial state of charge, the total solid concentration in the particle can be calculated by re-arranging the previous equations as follows:

$$\begin{aligned} c_T = c_{s,p_{avg}} * \frac{4}{3}\pi(R_s - \Delta r)^3 \\ = \left(\frac{SOC}{100} * \left(\theta_{p100\%} - \theta_{p0\%}\right) + \theta_{p0\%}\right) \\ * c_{s,max,p} * \frac{4}{3}\pi(R_s - \Delta r)^3 \end{aligned} \quad (41)$$

The next step is to evaluate lithium concentration values at various shells at steady state conditions (i.e.: assuming no diffusion). The total lithium concentration is divided equally among all shells as follows:

$$\begin{aligned} c_T = \sum_{i=1}^{M_r-1} r_i^2 4\pi\Delta r \\ = r_1^2 * 4\pi\Delta r c_1 + r_2^2 * 4\pi\Delta r c_2 \\ + r_3^2 * 4\pi\Delta r c_3 \dots r_{M_{r-1}}^2 \\ * 4\pi\Delta r c_{M_r-1} \end{aligned} \quad (42)$$

In order to evaluate the values of lithium concentrations at various shells $[c_1\ c_2\ c_3 \dots c_{Mr-1}]$, we use the final value theorem to evaluate the steady state concentration values. The technique is describes in details in the following subsections:

B. Initial concentration using Final Value Theorem

Given a dynamic system representing the lithium diffusion in the solid particle defined in state-space which is previously defined in equations (19-20). Where, matrices A and B can be written as follows:

$$A = \alpha_1 \begin{bmatrix} -2 & 2 & 0 & & & 0 & \\ 1/2 & -2 & 3/2 & \cdots & & 0 & \\ 0 & 2/3 & -2 & & & 0 & \\ & \vdots & & \ddots & & \vdots & \\ & & & & -2 & \frac{M_r-2}{M_r-3} & 0 \\ 0 & 0 & 0 & \cdots & \frac{M_r-3}{M_r-2} & -2 & \frac{M_r-1}{M_r-2} \\ & & & & 0 & \frac{M_r-2}{M_r-1} & \frac{2-M_r}{M_r-1} \end{bmatrix}$$

$$B = \alpha_2 \begin{bmatrix} 0 \\ 0 \\ \vdots \\ -\left(\frac{M_r}{M_r-1}\right) \end{bmatrix}$$

Assuming a zero input $u(t) = 0$, the zero-input solution can be formulated as follows:

This article has been accepted for publication in a future issue of this journal, but has not been fully edited. Content may change prior to final publication. Citation information: DOI 10.1109/JESTPE.2014.2331059, IEEE Journal of Emerging and Selected Topics in Power Electronics

$$\frac{dc}{dt} = Ac(t) \tag{43}$$

Taking unilateral Laplace transform,

$$sc(s) - c(0) = Ac(s) \tag{44}$$

Where $c(0) = c(t)$ at $t = 0$. Thus,

$$(sI - A)c(s) = c(0) \tag{45}$$

By applying the inverse, the states $c(s)$ can be evaluated as follows:

$$c(s) = (sI - A)^{-1}c(0) \tag{46}$$

By applying the Final value theorem for a unilateral transfer function $F(s)$ as follows:

$$Final\ Value = \lim_{t\to 0} f(t) = \lim_{s\to 0} sF(s) \tag{47}$$

Thus substituting (46) into (47), get:

$$Final\ Value = \lim_{t\to 0} f(t) = \lim_{s\to 0} s((sI - A)^{-1}c(0)) \tag{48}$$

The final value calculated above is function of the matrix A. It is clear that the matrix depends solely in the number of spherical shells M_r thus the final value depends on the number of shells. The final value achieved using the final value theorem represents the fraction by which the concentration will be equally divided among all shells. In this paper, this value is referred to as the $c_{s_{factor}}$. Accordingly, in order to evaluate the solid concentration in each spherical shell, assume that all lithium contained in the sphere is concentrated at the outermost shell. Then the following equation can be used:

$$\begin{aligned} c_i &= c_T/(r_{M_{r-1}}^2 * 4\pi\Delta r) * c_{s_{factor}} \\ &= \sum_{i=1}^{M_r-1} r_i^2 4\pi\Delta r c_i/(r_{M_{r-1}}^2 * 4\pi\Delta r) \\ &* c_{s_{factor}} \\ &= (r_1^2 * 4\pi\Delta r c_1 + r_2^2 * 4\pi\Delta r c_2 + r_3^2 \\ &* 4\pi\Delta r c_3 \ldots + r_{M_{r-1}}^2 \\ &* 4\pi\Delta r c_{M_r-1})/(r_{M_{r-1}}^2 * 4\pi\Delta r) \\ &* c_{s_{factor}} \end{aligned} \tag{49}$$

Where c_i represents the steady state initial concentration at every shell, for a given state of charge and the number of shells in the spherical particle.

C. Number of shells, SOC slope, and $c_{s_{factor}}$ relationship

By examining the state transition matrix A, a relationship between the numbers of electrode spherical shells (M_r) and the $c_{s_{factor}}$ can be derived. Assume that the number of spherical shells is $M_r = 3$, the state transition matrix can be formulated as function of M_r as follows:

$$A|_{M_r=3} = \begin{bmatrix} -2 & (M_r-1)/(M_r-2) \\ (M_r-2)/(M_r-1) & -(M_r-2)/(M_r-1) \end{bmatrix} \tag{50}$$

By converting from the state space to the transfer function representation, assuming zero input current. The transfer function (TF) for the outermost shell that relates the input butler-Volmer current to the subsequent inner shell can be written as follows:

$$TF|_{M_r=3} = \frac{(M_r-1)(s+2)}{(M_r-1)s^2 + (3M_r-4)s + M_r - 3} \tag{51}$$

By applying the final value theorem (47) and simplify get:

$$Final\ Value|_{M_r=3} = c_{s_{factor}}|_{M_r=3} = 1 - \frac{M_r-2}{3M_r-4} \tag{52}$$

Similarly, by repeating the same procedure for number of spherical shells $M_r = 4$, the state transition matrix can be formulated as function of M_r as follows:

$$A|_{M_r=4} = \begin{bmatrix} -2 & \frac{(M_r-2)}{(M_r-3)} & 0 \\ \frac{(M_r-3)}{(M_r-2)} & -2 & \frac{(M_r-1)}{(M_r-2)} \\ 0 & \frac{(M_r-2)}{(M_r-1)} & -\frac{(M_r-2)}{(M_r-1)} \end{bmatrix} \tag{53}$$

The transfer function (TF) for the outermost shell that relates the input current to the subsequent inner shell is as follows:

$$\begin{aligned} &TF|_{M_r=4} \\ &= \frac{(M_r-1)(s^2+4s+3)}{(M_r-1)s^3 + (5M_r-6)s^2 + (6M_r-10)s + M_r - 4} \end{aligned} \tag{54}$$

By applying the final value theorem and simplifying get:

$$Final\ Value|_{M_r=4} = c_{s_{factor}}|_{M_r=4} = 1 - \frac{3M_r-7}{6M_r-10} \tag{55}$$

Finally, for the number of spherical shells $M_r = 5$, the state transition matrix is:

This article has been accepted for publication in a future issue of this journal, but has not been fully edited. Content may change prior to final publication. Citation information: DOI 10.1109/JESTPE.2014.2331059, IEEE Journal of Emerging and Selected Topics in Power Electronics

$$A|_{M_r=5}=\begin{bmatrix} -2 & \frac{(M_r-3)}{(M_r-4)} & 0 & 0 \\ \frac{(M_r-4)}{(M_r-3)} & -2 & \frac{(M_r-2)}{(M_r-3)} & 0 \\ 0 & \frac{(M_r-3)}{(M_r-2)} & -2 & \frac{(M_r-1)}{(M_r-2)} \\ 0 & 0 & \frac{(M_r-2)}{(M_r-1)} & -\frac{(M_r-2)}{(M_r-1)} \end{bmatrix} \quad (56)$$

And the transfer function (TF) for is as follows:

$$TF|_{M_r=5}=\frac{(M_r-1)(s^3+6s^2+10s+4)}{(M_r-1)s^4+(7M_r-8)s^3+(15M_r-21)s^2+(10M_r-20)s+M_r-5} \quad (57)$$

By applying the final value theorem and simplify get:

$$Final\ Value|_{M_r=5}=c_{s_{factor}}|_{M_r=3}=1-\frac{6M_r-16}{10M_r-20} \quad (58)$$

By further examining the $c_{s_{factor}}$ values for various number of shells, the following relationship can be formulated:

$$c_{s_{factor}}=\frac{(\frac{M_r^2-3M_r+2}{2})(M_r)-(\frac{M_r^3-7M_r+6}{6})}{\left(\frac{M_r^2-M_r}{2}\right)(M_r)-(\frac{M_r^3-M_r}{6})} \quad (59)$$

Therefore the closed form of the relationship can be simplified to:

$$c_{s_{factor}}=1-\frac{2M_r^3-9M_r^2+13M_r-6}{2M_r^3-3M_r^2+M_r} \quad (60)$$

The relationship between the $c_{s_{factor}}$ and number of spherical shells (M_r) is as shown in Fig. 15:

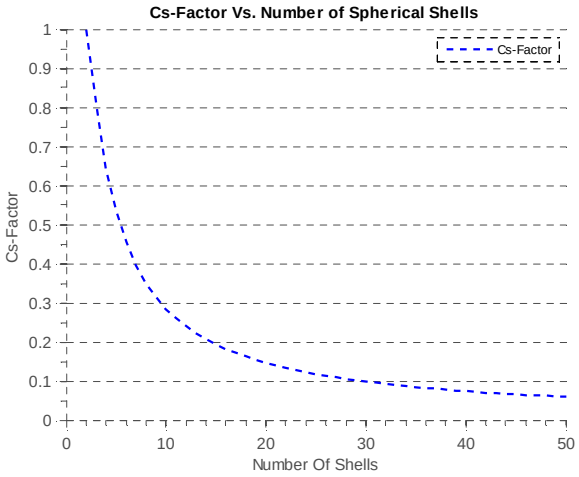

Fig. 15. Relationship between the $c_{s_{factor}}$ and the number of electrode spherical shells

By simulating the model using various number of shells, we can derive a relationship between the number of shells (M_r), the $c_{s_{factor}}$, and the slope of the SOC ($\Delta SOC/\Delta t$) curve as summarized in the following table:

TABLE 3.
MODEL SIMULATION PARAMETERS USING VARIOUS NUMBER OF SHELLS

$c_{s_{factor}}$	M_r	$\Delta SOC/\Delta t$	$(\Delta SOC/\Delta t)/c_{s_{factor}}$
0.26	11	2.72	10.5
0.13	21	2.85	20.5
0.12	25	2.88	24.5
0.09	31	2.90	30.5

As shown in Table 3, by dividing $c_{s_{factor}}$ by the SOC slope ($\Delta SOC/\Delta t$), a relationship which depends solely on the number of shells can be derived as follows:

$$(\Delta SOC/\Delta t)/c_{s_{factor}}=(2M_r-1)/2 \quad (61)$$

The previous relationship is of critical importance to scale the battery input current (I) to the Butler -Volmer current (J_p). This relationship is expanded upon to include dependence on the battery capacity (Q_{max}) in Ampere-second, normalized concentrations ($\theta_{p_{0\%}}, \theta_{p_{100\%}}$), particle radius ($R_s$), maximum positive solid concentration ($c_{s_{max}}$), and α_2.

$$(\Delta SOC/\Delta t)/c_{s_{factor}}=(\frac{2M_r-1}{2}*\alpha_2*\Delta r)/(c_{s_{max}}*R_s*Q_{max}*(\theta_{p_{100\%}}-\theta_{p_{0\%}})) \quad (62)$$

Where,

$$\alpha_1=D_s/\delta r^2 \text{ and } \alpha_2=1/(Fa_s\Delta r)$$

The relation is further expanded to involve volumetric average used for SOC calculation:

$$\left(\frac{\Delta SOC}{\Delta t}\right)/c_{s_{factor}}=((\frac{2M_r-1}{2})*\left(\frac{M_r}{M_r-1}\right)^3*\alpha_2*\Delta r)/(c_{s_{max}}*R_s*Q_{max}*(\theta_{p_{100\%}}-\theta_{p_{0\%}})) \quad (63)$$

The aforementioned relationship is used as an optimization constraint. The optimizer is used to optimize the electrode area (A) and then using the previous constraint to calculate the electrode thickness δ as follows:

This article has been accepted for publication in a future issue of this journal, but has not been fully edited. Content may change prior to final publication. Citation information: DOI 10.1109/JESTPE.2014.2331059, IEEE Journal of Emerging and Selected Topics in Power Electronics

$$\delta = \left(\frac{1}{A}\right) * \left(\left(\frac{2M_r - 1}{2}\right) * \left(\frac{M_r}{M_r - 1}\right)^3 * \alpha_2 * \Delta r * \ c_{s_{factor}} \right) / (c_{s_{max}} * R_s * Q_{max} * (\theta_{p_{100\%}} - \theta_{p_{0\%}}) \quad (64)$$

This relationship indicates that capacity degradation due to battery aging is attributed to a decreased sphere effective volume.

VI. Parameters Optimization

A benchmark Urban Dynamometer Driving Schedule has been used for data fitting. Experimental data from LiFePO4 cells have been collected and fitted to the reduced-order model. Even though the reduced-order model has fewer parameters compared to the full-order model, model parameters are still difficult to identify. Accordingly, in this work, the full-set of the reduced-order model parameters are being attained using genetic algorithm optimization.

A. Parameters to be optimized

The full-set of the reduced order electrochemical battery model parameters have been identified. The 18 parameters are as follows: the solid maximum particle concentration in the anode and cathode ($c_{s,max,p}, c_{s,max,n}$), positive and negative diffusion coefficients ($D_{s,p}, D_{s,n}$), positive and negative active surface area per electrode ($a_{s,p}, a_{s,n}$), positive and negative electrode area (A), electrode film resistance (R_{SEI}) (also known as the solid electrolyte interface resistance), maximum positive and negative solid normalized concentrations (stoichiometry values) ($\theta_{p_{100}}, \theta_{n_{100}}$), minimum positive and negative normalized solid concentration ($\theta_{p_0}, \theta_{n_0}$), anode and cathode particle radiuses (R_{s_p}, R_{s_n}), active material volume fraction ($e_{s,p}, e_{s,n}$), average electrolyte concentration ($\bar{c}_e$), and positive and negative current coefficient or reaction rate (k_0). Some parameters are held constant as shown in Table 4.

TABLE 4.
FIXED MODEL PARAMETERS (HELD CONSTANT DURING OPTIMIZATION)

PARAMETER NAME (UNIT)	PARAMETER VALUE
Change transfers coefficient $\boldsymbol{\alpha_a}, \boldsymbol{\alpha_c}$	0.5,0.5
Universal gas constant ($\boldsymbol{J\ K^{-1}\ mol^{-1}}$)	8.3144 e+4
Temperature ($\boldsymbol{°K}$)	298.15
Faraday's constant ($\boldsymbol{C\ mol^{-1}}$)	96485

B. Genetic Algorithm optimization Technique

Genetic algorithm is an adaptive technique that is based on heuristic search and uses evolution to direct the search to regions of better performance (minimum error). It is best suited for complex problems in which obtaining a gradient is rather difficult to attain. A detailed illustration of genetic algorithms can be found in references [21, 22]. A brief summary of the Genetic Algorithm optimization used in this paper is summarized below [23]:

1. ***Creation of random initial population***

   In this work, 1000 individuals have been used for every population. The initial range is set as illustrated in Table 5. An initial guess based on literature parameters values and the authors' best knowledge has been adopted in this work.

2. ***Generating a sequence of new populations as follows:***

   - *Evaluate the fitness value of each population member and scale the raw fitness values to generate an operational range of values.*
   - *Select individuals based on their fitness function, these individuals are called parents.*
   - *Generate children from the parents, wither by crossover or mutation.*
   - *Replace individuals from current population with children to from the next generation.*

3. ***The algorithm repeats until one of the stopping criteria is reached.***

C. Results and Discussion

During optimization, bounds have been set on all 18 parameters to be optimized based on the authors' best knowledge. Bounds for each parameter are as shown in Table 5. In order to identify the electrochemical model parameters using Genetic Algorithm, an objective function has to be selected. The parameter identification objective function used in this research is targeted at minimizing the error between the model output terminal voltage $\hat{V}(t)$ and the experimentally measured terminal voltage $V(t)$. The objective function is a cumulative sum of the squared voltage error as follows:

$$min \int_0^T \left(V(t) - \hat{V}(t)\right)^2 dt \quad (65)$$

The Urban Dynamometer Driving Schedule (UDDS) has been used for parameters fitting. The UDDS driving cycle has been selected since it entails fast changing signal, rich in its frequency content thus favored when optimization strategies are applied. The driving cycle includes resting periods thus captures the battery relaxation effects. In addition, the cycle includes charging current that represents regenerative braking in addition to discharging currents representing vehicle acceleration. The driving cycle has been previously used to get the electrochemical battery model parameters for the full-order electrochemical model in previous publication [5]. As shown in the paper, the model will be validated using other driving cycles (HWFET, US06) that has never been used during

This article has been accepted for publication in a future issue of this journal, but has not been fully edited. Content may change prior to final publication. Citation information: DOI 10.1109/JESTPE.2014.2331059, IEEE Journal of Emerging and Selected Topics in Power Electronics

parameters extraction process and the model exhibits good accuracy. The Genetic algorithm starts varying the 18 model parameters to be identified. The genetic algorithm is best suited in this application since gradient information is hard to evaluate for the electrochemical model.

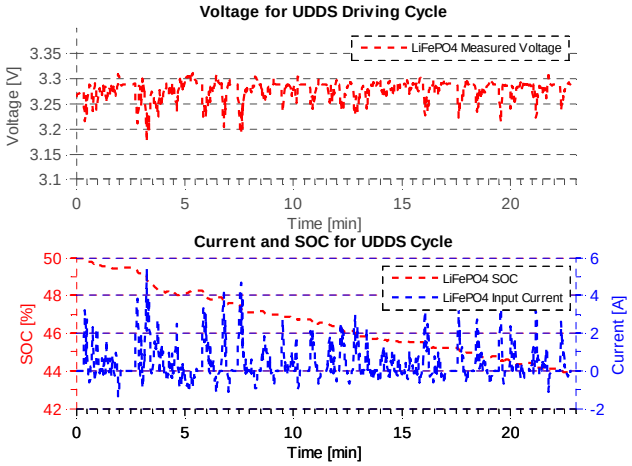

Fig. 16. Battery Voltage (Upper Figure), SOC and Current (Bottom Figure) for one UDDS Cycle

The scaled current input from an Urban Dynamometer Driving cycle has been used as an input to the model along with the parameter guess generated from the GA algorithm.

The current is scaled down by a factor of 15 assuming 15 cells are connected in parallel, also, cell balancing is ignored in this context. Current, voltage, and SOC data from a UDDS cycle are as shown in Fig. 16 (assuming positive current for discharge and negative current for charge). The model is simulated once for every member of the population and the terminal voltage is further compared with the experimental terminal voltage. Since overpotential equations (29) and (30) used for terminal voltage calculation involve square root calculation, it might generate complex numbers, thus points that generate complex terminal voltage has been penalized by setting the terminal voltage to a very large number.

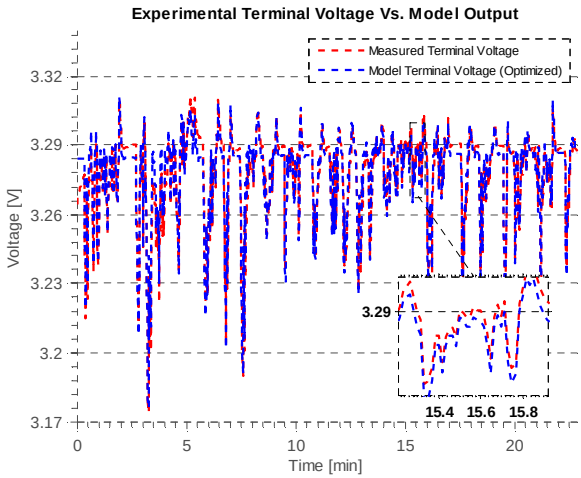

Fig. 17. Electrochemical Battery Model vs. Experimental Data from a UDDS Driving Cycle

The genetic algorithm optimization has been set to 10 runs and to 1000 population size due to extensive computational complexity required by the algorithm. The algorithm has been conducted on a mobile workstation with 3.0 GHz, quad Core i7-3940XM Extreme Edition processor.

TABLE 5.
ELECTROCHEMICAL BATTERY MODEL OPTIMIZER BOUNDS

PARAMETER NAME (ELECTRODE) (SYMBOL) (UNIT)	LOWER BOUND	UPPER BOUND
Maximum solid-phase concentration (Positive) $(\boldsymbol{C_{s,max,p}})$ $(\boldsymbol{mol/cm^3})$	1e-4	0.1
Maximum solid-phase concentration (Negative) $(\boldsymbol{C_{s,max,n}})$ $(\boldsymbol{mol/cm^3})$	1e-4	0.1
Solid phase diffusion coefficient (Positive) $(\boldsymbol{D_{s,p}})$ $(\boldsymbol{cm^2/sec})$	1e-15	1e-8
Solid phase diffusion coefficient (Negative) $(\boldsymbol{D_{s,n}})$ $(\boldsymbol{cm^2/sec})$	1e-15	1e-8
Active surface area per electrode unit volume (Positive) $(\boldsymbol{a_{s,p}})$	10000	180000
Active surface area per electrode unit volume (Negative) $(\boldsymbol{a_{s,n}})$	10000	130000
Maximum solid concentration (Positive) $(\boldsymbol{\theta_{p_{100\%}}})$	0	1
Minimum solid concentration (Positive) $(\boldsymbol{\theta_{p_{0\%}}})$	0	1
Maximum solid concentration (Negative) $(\boldsymbol{\theta_{n_{100\%}}})$	0	1
Minimum solid concentration (Negative) $(\boldsymbol{\theta_{n0\%}})$	0	1
Particle radius (Positive) $(\boldsymbol{R_{s,p}})$ $(\boldsymbol{cm})$	1e-7	1e-1
Particle radius (Negative) $(\boldsymbol{R_{s,n}})$ $(\boldsymbol{cm})$	1e-7	1e-1
Active material volume fraction (Positive) $(\boldsymbol{e_{s,p}})$	0	1
Active material volume fraction (Negative) $(\boldsymbol{e_{s,p}})$	0	1
Reaction rate $(\boldsymbol{k_0})$	1000	12000
Solid Electrolyte interface Resistance $(\boldsymbol{R_{SEI}})$ $(\boldsymbol{\Omega})$	0	1
Average electrolyte concentration $(\boldsymbol{\bar{c}_e})$ $(\boldsymbol{mol/cm^3})$	1e-5	1e-1
Electrode plate area (Positive, Negative) (A) $(\boldsymbol{cm^2})$	100	20000

The estimated value of the $\boldsymbol{R_{SEI}}$ inherently includes current collectors and electrolyte resistance. The algorithm requires approximately 6 hours to generate the optimized parameters. The optimized values generated by the genetic algorithm technique are summarized in

Table 6.

As shown in Fig. 17, the optimized electrochemical battery model output fits the experimental data quite well.

This article has been accepted for publication in a future issue of this journal, but has not been fully edited. Content may change prior to final publication. Citation information: DOI 10.1109/JESTPE.2014.2331059, IEEE Journal of Emerging and Selected Topics in Power Electronics

The slight shift is due to the averaging of the OCV and SOC relationship and due to the approximations from the full-order to the reduced-order form. Recall that the model assumes constant electrolyte concentration and only one representative particle for each electrode.

TABLE 6.
ELECTROCHEMICAL BATTERY MODEL OPTIMIZED PARAMETERS

PARAMETER NAME (ELECTRODE) (SYMBOL) (UNIT)	OPTIMIZED PARAMETERS
Maximum solid-phase concentration (Positive) ($C_{s,max,p}$) (mol/cm^3)	0.04782
Maximum solid-phase concentration (Negative) ($C_{s,max,n}$) (mol/cm^3)	0.08147
Solid phase diffusion coefficient (Positive) ($D_{s,p}$) (cm^2/sec)	7.432474 e-09
Solid phase diffusion coefficient (Negative) ($D_{s,n}$) (cm^2/sec)	1.139458 e-09
Active surface area per electrode unit volume (Positive) ($a_{s,p}$)	164083.82
Active surface area per electrode unit volume (Negative) ($a_{s,n}$)	65588.80
Maximum solid concentration (Positive) ($\theta_{p_{100\%}}$)	0.9149
Minimum solid concentration (Positive) ($\theta_{p_{0\%}}$)	0.6976
Maximum solid concentration (Negative) ($\theta_{n_{100\%}}$)	0.3101
Minimum solid concentration (Negative) ($\theta_{n_{0\%}}$)	0.1535
Particle radius (Positive) ($R_{s,p}$) (cm)	0.0015
Particle radius (Negative) ($R_{s,n}$) (cm)	0.0264
Active material volume fraction (Positive) ($e_{s,p}$)	0.1646
Active material volume fraction (Negative) ($e_{s,n}$)	0.7970
Reaction rate (k_0)	10016.583
Solid Electrolyte interface Resistance (R_{SEI}) (Ω)	0.0104
Average electrolyte concentration ($\bar{c}_e$) (mol/cm^3)	0.0851
Electrode plate area (Positive, Negative) (A) (cm^2)	16524.27

The root mean square error (RMSE) between the measured terminal voltage ($V(t)$) and the electrochemical model output ($\hat{V}(t)$) for n number of samples can be calculated as follows:

$$RMSE = \sqrt{\frac{\sum_{t=1}^{n} V(t) - \hat{V}(t)}{n}} \quad (66)$$

The error between experimental and the ECM model output is shown in Fig. 18. Using the optimized battery model parameters, the RMSE for a UDDS cycle is 0.22057 mV.

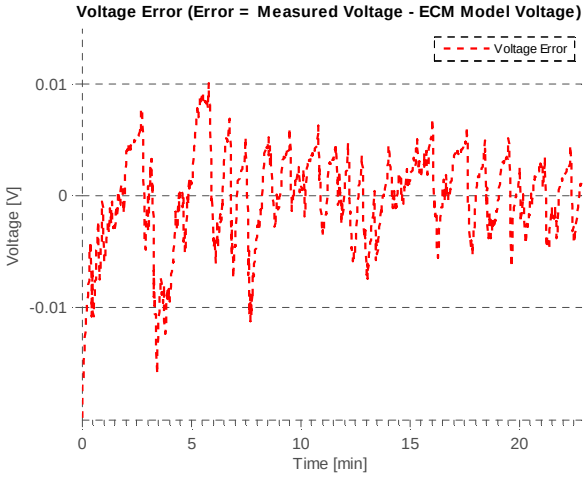

Fig. 18. Voltage Error between experimental and ECM Output

The actual battery SOC Vs. electrochemical battery model output SOC based on spherical average are shown in Fig. 19. The actual SOC is calculated using coulomb counting provided by the Arbin cycler.

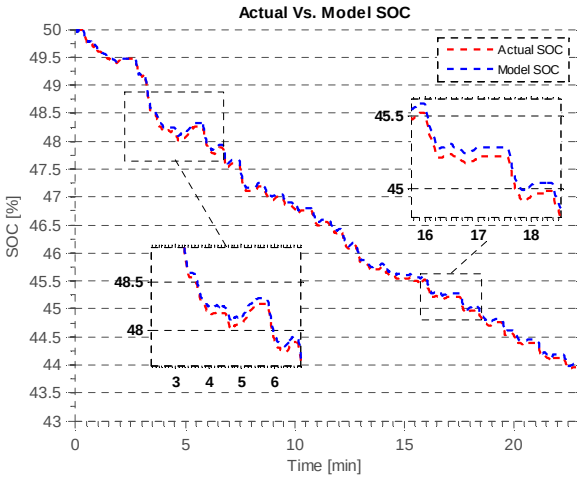

Fig. 19. Actual SOC (using Coulomb Counting) Vs. Model SOC

The SOC has been reset before conducting the test to minimize accumulated error due to integration. The histogram of the voltage error is shown in Fig. 20. As shown, the maximum absolute error is within 0.02 V which indicates that the model is very accurate using the optimized parameter values at this specific state of life. As battery ages, model parameters will significantly change and will result in model deviation.

This article has been accepted for publication in a future issue of this journal, but has not been fully edited. Content may change prior to final publication. Citation information: DOI 10.1109/JESTPE.2014.2331059, IEEE Journal of Emerging and Selected Topics in Power Electronics

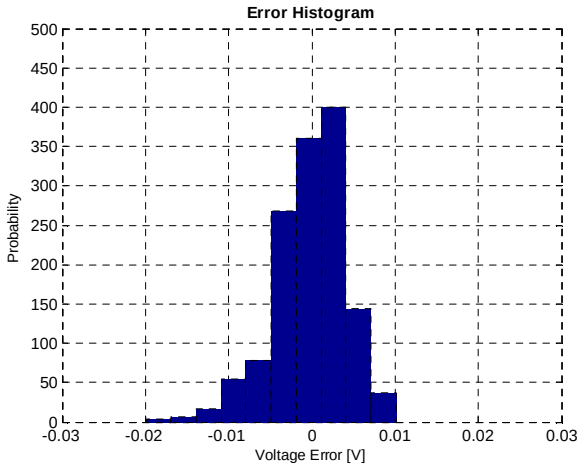

Fig. 20. Probability density plot of voltage error for UDDS cycle

One of the major advantages of electrochemical modeling in comparison to the equivalent circuit-based models is that a further insight into lithium concentrations in both electrodes can be monitored. As shown in Fig. 21, the solid-electrolyte interface concentration in the cathode and the anode for a UDDS cycle is presented.

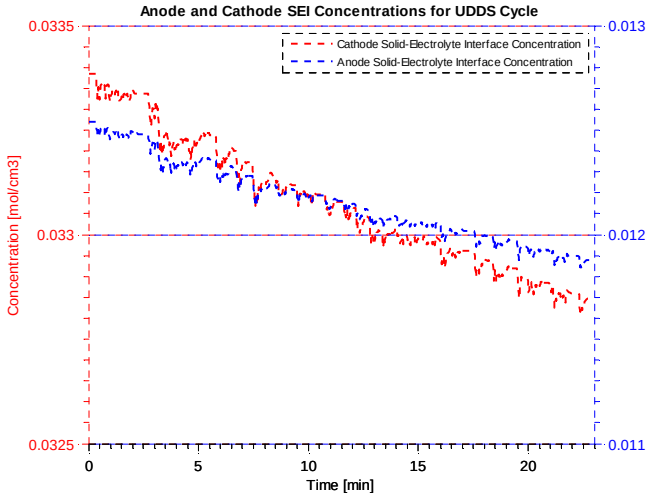

Fig. 21. Anode and Cathode Lithium Concentrations at the Solid-Electrolyte Interface

Furthermore, Fig. 22 shows the variations of lithium concentrations across various shells (10 shells) in the cathode for the UDDS cycle. It is clear that the solid-electrolyte interface concentrations is rapidly varying since it is directly related to the terminal voltage concentrations, while the other inner shells are slowly varying since they are not directly exposed to the Butler-Volmer current. This describes the fact that the battery exhibits relaxation effects for zero current input which is related to the variation of lithium concentration at the surface, as it decays to the inner shells over time. The total sphere concentration is held constant for zero input current and accordingly the battery state of charge is fixed.

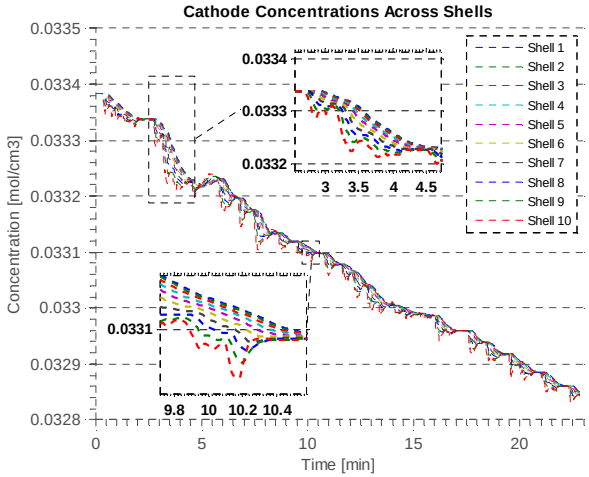

Fig. 22. Lithium Concentration in the Cathode across Various Shells

D. *Model validation*

The optimized model along with the developed SOC parameterization strategy has been validated using other real-world driving cycles that have never been seen by the model. Current profiles from highway fuel economy test (HWFET) and a light duty drive cycle for high speed and high load (US06) driving cycles have been used. As shown in Fig. 23 and Fig. 24, the optimized model parameters using UDDS cycle still generates good results. The RMSE for terminal voltage and SOC using the US06 driving cycle are 0.0041531 V and 0.2932 % respectively.

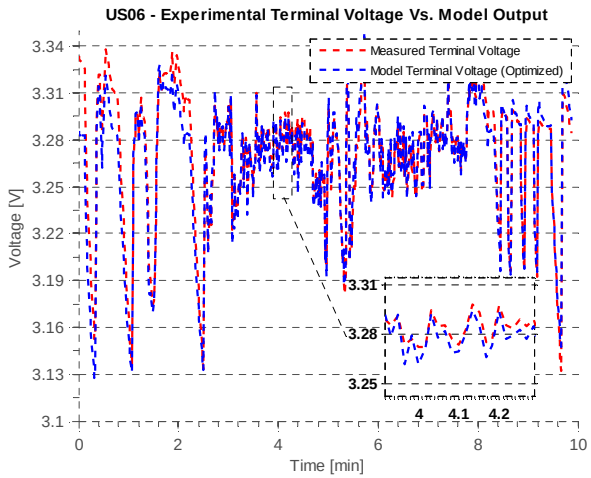

Fig. 23. Electrochemical Battery Model vs. Experimental Data from a US06 Driving Cycle

As shown in Fig. 25, the model has also been validated using a HWFET driving cycle, since this driving cycle has never been seen during model fitting, a slight offset between the model and the measured voltage has been exhibited. This is also due to the approximation done during model reduction process from a full-order to a reduced-order form. The offset is due to the averaging process of both charging/discharging SOC-OCV curves.

This article has been accepted for publication in a future issue of this journal, but has not been fully edited. Content may change prior to final publication. Citation information: DOI 10.1109/JESTPE.2014.2331059, IEEE Journal of Emerging and Selected Topics in Power Electronics

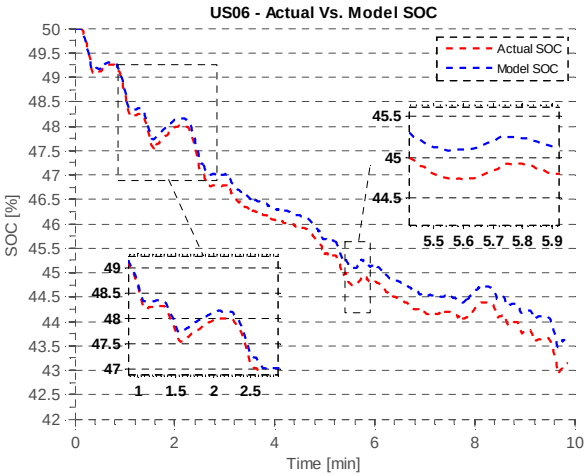

Fig. 24. Actual SOC (using Coulomb Counting) Vs. Model SOC for US06 Driving Cycle

The maximum voltage offset is approximately 0.03 V and the RMSE across the entire driving cycle is 0.0154 V which is relatively small. The ECM model SOC Vs. actual SOC (from the Arbin cycler) are as shown in Fig. 26, The RMSE for the SOC using the HWFET driving cycle is 0.161 %.

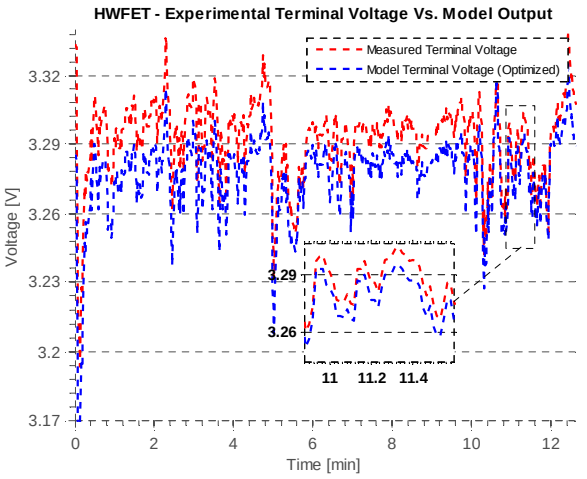

Fig. 25. Electrochemical Battery Model vs. Experimental Data from a HWFET Driving Cycle

Since these driving cycles have never been utilized during optimization, the RMSE is slightly higher compared to the UDDS cycle. However, the results for terminal voltage and SOC are within the acceptable range of operation. A summary of the terminal voltage and SOC RMSE for all driving cycles used are shown in Fig. 27. It is clear that since the UDDS cycle has been used for parameters fitting, it generates the least error for both the voltage and the SOC. The HWFET exhibits the highest voltage error while the US06 demonstrates the highest error on SOC.

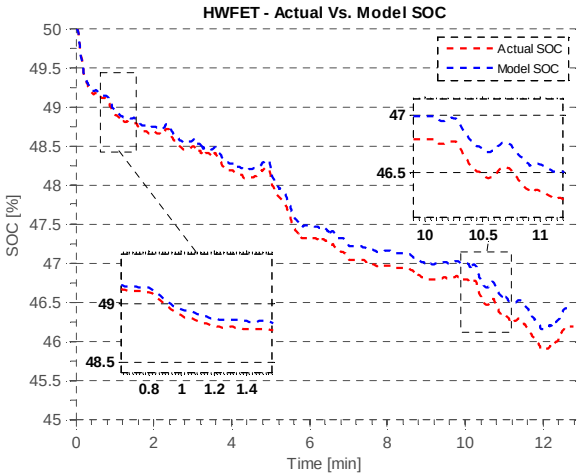

Fig. 26. Actual SOC (using Coulomb Counting) Vs. Model SOC for HWFET Driving Cycle

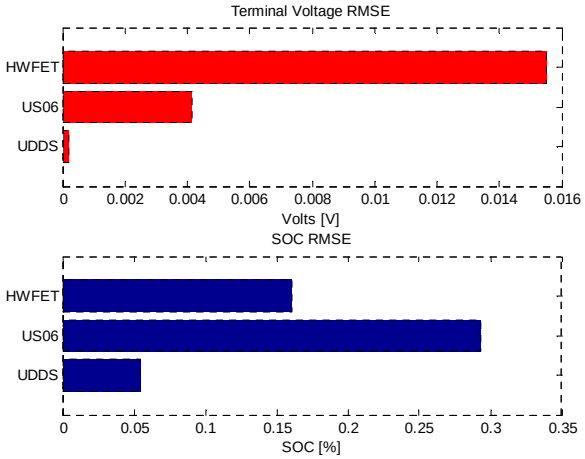

Fig. 27. Terminal voltage (upper) and SOC RMSE (lower) for all driving cycles

VII. Conclusions

In this paper, identification of 18 model parameters of the reduced-order electrochemical model using genetic algorithm has been conducted. The technique can be used for a non-invasive determination of the electrochemical model parameters for any battery chemistry. Furthermore, a SOC parameterization model has been developed and effectively utilized as a constraint during parameters optimization process. The electrochemical model with optimized parameters fits voltage experimental data very well with an RMSE of approximately 0.2 mV. Moreover, spherical average concentration can be effectively used for SOC calculation provided that the initial SOC is known.

The reduced-order model results in heavy loss of information from the full-order model. However, it still maintains a strong connection to the internal battery potential and diffusion dynamics which is beneficial for the state of health estimation. Future research involves extension of the proposed methodology to incorporate changes of aging

This article has been accepted for publication in a future issue of this journal, but has not been fully edited. Content may change prior to final publication. Citation information: DOI 10.1109/JESTPE.2014.2331059, IEEE Journal of Emerging and Selected Topics in Power Electronics

parameters using correlation with ampere-hour throughput and other aging parameters such as battery discharge rate, temperatures, and depth of discharge.

APPENDIX

The full order electrochemical battery model is illustrated in this section. Diffusion dynamics in one dimensional (1-D), single axis (X-axis) is only considered while diffusion dynamics in both dimensions (Y-axis and Z-axis) are ignored [24, 25]. The state variables required to describe the 1D-spatial model at any x, t are the electric potential in the solid electrode $\phi_s(x,t)$, the electric potential in the electrolyte $\phi_e(x,t)$, the lithium concentration in the solid phase $c_s(x,r,t)$ and the lithium concentration in the electrolyte $c_e(x,t)$. Mathematical equations to model the electrochemical behavior of a Li-ion battery is presented below, the input to the model is the external current *I* applied to the battery, and the output of the model is the corresponding output voltage V [26]. The 1D-spatial electrochemical model consists of four PDEs [27], the solid and electrolyte potentials are described by the following two equations [24, 25]:

$$\frac{\partial}{\partial x}k^{eff}\frac{\partial}{\partial x}\emptyset_e + \frac{\partial}{\partial x}k_D^{eff}\frac{\partial}{\partial x}\ln c_e = -j^{Li} \quad \text{(A1)}$$

$$\frac{\partial}{\partial x}\sigma^{eff}\frac{\partial}{\partial x}\emptyset_s = j^{Li} \quad \text{(A2)}$$

The diffusion of lithium in the electrolyte is modeled using Fick's law for linear coordinates as shown by equation (A3),

$$\frac{\partial \varepsilon_e c_e}{\partial t} = \frac{\partial}{\partial x}\left(D_e^{eff}\frac{\partial c_e}{\partial x}\right) + \frac{1-t^0}{F}j^{Li} \quad \text{(A3)}$$

While the solid (electrode) phase diffusion is modeled by Fick's laws of diffusion for spherical coordinates as shown in equation (A4):

$$\frac{\partial c_s}{\partial t} = \frac{\partial}{\partial r}(D_s\frac{\partial c_s}{\partial r}) \quad \text{(A4)}$$

In order to simplify the model, the electrolyte concentration (c_e) is assumed to be constant. This approximation will greatly simplify the model while preserving accuracy of <5% compared to the detailed model [9]. After simplification, equation (A3) is removed, equations (A2) and (A4) remain unchanged, and equation (A1) is being simplified as follows:

$$\frac{\partial}{\partial x}\mathrm{k^{eff}}\frac{\partial}{\partial x}\emptyset_e = -\mathrm{j^{Li}} \quad \text{(A5)}$$

Equations (A6) and (A7) introduce the solid current density (i_s) ($\mathrm{A/cm^2}$) and the electrolyte current density (i_e) ($\mathrm{A/cm^2}$):

$$i_e(x) = -k^{eff}\frac{\partial}{\partial x}\emptyset_e \quad \text{(A6)}$$

$$i_s(x) = -\sigma^{eff}\frac{\partial}{\partial x}\emptyset_s \quad \text{(A7)}$$

Thus, the solid and electrolyte potential equations (A1) and (A2) can be re-written as follows:

$$\frac{\partial}{\partial x}i_e(x) = j^{Li} \quad \text{(A8)}$$

$$\frac{\partial}{\partial x}i_s(x) = -j^{Li} \quad \text{(A9)}$$

The Butler-Volmer current density is described [24, 25]:

$$J^{Li} = a_s j_o[exp\left(\frac{\propto_a F}{RT}\eta\right) - exp(\frac{\propto_c F}{RT}\eta)] \quad \text{(A10)}$$

Where R and F are the universal gas constant and Faraday's constant, T is the absolute temperature and η is the over potential [24, 25].

$$\eta = \emptyset_s - \emptyset_e - U(c_{se}) \quad \text{(A11)}$$

In equation (A11), U is the open circuit voltage which is a function of the lithium concentration at the solid-electrolyte interface $c_{se}(x,t) = c_s(x,R_s,t)$. The concentration at the interface between the solid and the electrolyte is related to the critical surface charge (CSC):

$$CSC(t) = \frac{\theta - \theta_{0\%}}{\theta_{100\%} - \theta_{0\%}} \quad \text{(A12)}$$

By defining the normalized solid-electrolyte concentration θ as follows:

$$\theta = \frac{solid - electrolyte\ concentration}{maximum\ solid\ concentration} = \frac{c_{se}}{c_{s,max}} \quad \text{(A13)}$$

Where, $\theta_{0\%}$ and $\theta_{100\%}$ are the normalized concentrations corresponding to 0% (fully discharged) and 100% (fully charged). $\theta_{100\%}$ can be defined by obtaining the concentration corresponding to the maximum fully charged battery. Subsequently, the 0% reference value can be calculated by subtracting the battery capacity Q as [10]:

$$\theta_{0\%} = \theta_{100\%} - \frac{Q}{\delta}(\frac{1}{AF\varepsilon c_{s,max}}) \quad \text{(A14)}$$

The open circuit voltage varies from the cathode and the anode. An empirical relationship is used to relate the open circuit voltage to the normalized state of charge which is given by [28]:

$$\begin{aligned} U_n(\theta_n) = {} & 8.0029 + 5.064\theta_n - 12.578\theta_n^{0.5} \\ & - 8.6322 \times 10^{-4}\theta_n^{-1} + 2.176 \\ & \times 10^{-5}\theta_n^{\frac{3}{2}} \\ & - 0.46016\, exp[15(0.06 - \theta_n)] \\ & - 0.55364 exp[-2.4326(\theta_n \\ & - 0.92)] \end{aligned} \quad \text{(A15)}$$

For the positive electrode, the empirical equation is as follows [9]:

$$U_p(\theta_p) = 85.681\theta_p^6 - 357.7\theta_p^5 + 613.89\theta_p^4 - 555.65\theta_p^3 + 281.06\theta_p^2 - 76.648\theta_p + 13.1983 - 0.30987exp(5.657\theta_p^{115}) \quad \text{(A16)}$$

The coefficient j_o depends on the solid and electrolyte concentrations according to the following equations:

$$j_o = (c_e)^{\alpha_a}\left(c_{s,max} - c_{se}\right)^{\alpha_a}(c_{se})^{\alpha_c} \quad \text{(A17)}$$

The solid potential is related to the measured cell potential as follows [24, 25]:

$$V = \emptyset_s(x = L) - \emptyset_s(x = 0) - R_{SEI}I \quad \text{(A18)}$$

where R_{SEI} is the solid electrolyte interface (film) resistance at the electrode surface, this resistance increases after charging and discharging cycles (battery aging). As mentioned earlier, the full order model is relatively complex so further simplification is necessary to be useful for control and estimation purposes.

ACKNOWLEDGMENTS

Financial support from Ford Motor Company and NSERC (National Sciences and Engineering Research Council of Canada) is gratefully acknowledged. The authors would also like to thank researchers and engineers: Robyn Jackey, Javier Gazzarri, and Kevin Rzemien from MathWorks Inc. for their help with the electric vehicle model development and tuning.

REFERENCES

[1] J. LeSage, "Long-term maintenance costs show benefit of electric vehicles over ICEs," Green Auto Blog, 2012.

[2] C. Shiau, C. Samaras, R. Hauffe and J. Michalek, "Impact of battery weight and charging patterns on the economic and environmental benefits of plug-in hybrid vehicles," *Energy Policy*, vol. 37, no. 7, p. 2653–2663, 2009.

[3] S. E. Samadani, R. A. Fraser and M. Fowler, "A Review Study of Methods for Lithium-ion Battery Health Monitoring and Remaining Life Estimation in Hybrid Electric Vehicles," *SAE International* , 2012.

[4] C. Speltino, D. D. Domenico, G. Fiengo and A. Stefanopoulou, "Experimental identification and validation of an electrochemical model of a Lithium-Ion Battery," 2009.

[5] J. C. Forman, S. J. Moura, J. L. Stein and H. K. Fathy, "Genetic identification and fisher identifiability analysis of the Doyle–Fuller–Newman model from experimental cycling of a LiFePO4 cell," *Journal of Power Sources*, no. 210, pp. 263-275, 2012.

[6] "www.MathWorks.com/Matlabcentral/fileexchange," [Online].

[7] M. Doyle, T. Fuller and J. Newman, "Modeling of Galvanostatic Charge and Discharge of the Lithium/Polymer/insertion Cell," *Journal of Electrochemical Society* , vol. 140, pp. 1526-1533, 1993.

[8] D. Domenico, S. Anna and F. Giovanni, "Lithium-Ion Battery State of Charge and Critical Surface Charge Estimation Using an Electrochemical Model-Based Extended Kalman Filter," *Journal of Dynamic Systems, Measurement, and Control*, vol. 132, pp. 1-11, 2010.

[9] K. Smith and C. Y. Wang, "Solid-State Diffusion Limitations on Pulse Operation of a Lithium-Ion Cell for Hybrid Electric Vehicles," *Journal of Power Sources*, p. 628–639, 2006.

[10] D. D. Domenico, G. Fiengo and A. Stefanopoulou, "Lithium-Ion battery State of Charge estimation with a Kalman Filter based on a electrochemical model," *IEEE Interantional Conference on control Applications (CCA)*, pp. 702-707, 2008.

[11] "http://www.epa.gov/nvfel/testing/dynamometer.htm," U.S. EPA. [Online].

[12] R. E. Kruse and T. A. Huls, "Development of the Federal Urban Driving Schedule," May 14, 1973.

[13] "http://www.wired.com/autopia/2010/11/honda-finds-evs-a-perfect-fit," [Online].

[14] C. Hua, B. D. Younb and J. Chung, "A multiscale framework with extended Kalman filter for lithium-ion battery SOC and capacity estimation," 2012.

[15] "www.epa.gov/nvfel/testing/dynamometer.htm," EPA United States Environmental Protection Agency. [Online].

[16] U. D. o. Energy, "Plug-In Hybrid Electric Vehicle Value Proposition Study," U.S. Department of Energy, ORNL/TM-2010/46, July, 2010.

[17] "Battery Test Manual for Plug-In Hybrid Electric Vehicles," U.S. Department of Energy, Idaho National Laboratory, Idaho Falls, Idaho 83415, March 2008.

[18] G. L. Plett, "Extended Kalman filtering for battery management systems of LiPB-based HEV battery packs: Part 3. State and parameter estimation," *Journal of Power Sources*, no. 134, p. 277–292, 2004.

[19] Y. Fuentes. and M. Doyle , "Computer simulations of a lithium-ion polymer battery and implications for higher capacity next-generation battery designs," *Journal of Electrochemical Society*, vol. 150, p. A706–A713, 2003.

[20] C. Speltino, D. D. Domenico , F. Giovanni and A. Stefanopoulou, "Experimental identification and validation of an electrochemical model of a Lithium-Ion Battery".

[21] J. Holland, "Adaptation in Natural and Artificial Systems," *University of Michigan Press, Ann Arbor*, 1975.

[22] D. Goldberg, "Genetic Algorithms in search, Optimization, and MAchine Learning," *Addison-Wesley, Reading, Massachusetts*, 1989.

[23] M. Inc, "www.mathworks.com/help/grads/how-the-genetic-algorithm-works.html," 2013. [Online].

[24] J. Newman and W. Tiedemann, "Porous-electrode theory with battery applications," *AIChE Journal*, vol. 21, no. 1, pp. 25-41, 1975.

[25] A. J. Bard and L. R. Faulkner, "Electrochemical Methods: Fundamentals and Applications," *Russian Journal of Electrochemistry*, vol. 38, no. 12, 2002.

[26] N. Chaturvedi, R. Klein, J. Christensen, J. Ahmed and A. Kojic, "Algorithms for Advanced Battery-Management Systems Modeling, Estimation and Control Challenges for Lithium-ion Batteries," *IEEE CONTROL SYSTEMS MAGAZINE*, pp. 49-68, 2010.

[27] K. Smith and C.-Y. Wang, "Solid-state diffusion limitations on pulse operation of a lithium ion cell for hybrid electric vehicles," *Journal of Power Sources*, vol. 161, no. 1, pp. 628-639, 2006.

[28] M. Doyle and Y. and Fuentes, "Computer Simulations of a Lithium-Ion Polymer Battery and Implications for Higher Capacity Next-Generation Battery Designs," *Journal of Electrochemistry Society*, p. A706–A713, 2003.

Ryan is currently a PhD candidate at McMaster University, Canada. Ryan obtained his Masters of Applied Science (M.A.Sc) degree from McMaster University. Ryan has been active in the area of hybrid vehicles control, engine management and fault detection, and battery monitoring and control. Ryan was the recipient of best paper award at the IEEE Transportation

This article has been accepted for publication in a future issue of this journal, but has not been fully edited. Content may change prior to final publication. Citation information: DOI 10.1109/JESTPE.2014.2331059, IEEE Journal of Emerging and Selected Topics in Power Electronics

Electrification Conference and Expo (ITEC 2012), Michigan, USA. He is currently a Stanford Certified Project Manager (SCPM), certified Professional Engineer (P.Eng.) in Ontario, a member of the Green Auto Powertrain (GAPT) research team, and a student member of the Institute of Electrical and Electronics Engineers (IEEE).

Dr. Mohammed El Sayed obtained a B.Sc. in Mechanical Engineering from Helwan University, Egypt in 1999. He then earned a M.Sc. degree in Mechanical Engineering in 2003. Mohammed obtained his Ph.D. in 2012 in the areas of control theory and applied mechatronics. He is currently a registered member of the Professional Engineers of Ontario (PEO) and is currently working as a development engineer at Schaeffler Group, USA. Mohammed's research interests include: fluid power and hydraulics, state and parameter estimation, intelligent and multivariable control, actuation systems, and fault detection and diagnosis.

Ienkaran Arasaratnam received the B.Sc. degree (with first class honors) from the Department of Electronics and Telecommunication Engineering, University of Moratuwa, Sri Lanka, in 2003 and the M.A.Sc. and Ph.D. degrees from the Department of Electrical and Computer Engineering, McMaster University, Hamilton, ON, Canada, in 2006 and 2009, respectively. During his Ph.D., he developed the Cubature Kalman Filtering Algorithm for approximate nonlinear Bayesian estimation and patented its application to cognitive tracking radar systems. He is currently working as a Research and Development Engineer at Ford Motor Company in Windsor, ON, Canada. His current research focuses on electrified and intelligent transportation and energy harvesting technology.

Dr. Jimi Tjong is the Technical Leader and Manager of the Powertrain Engineering, Research & Development Centre (PERDC). It is a result oriented organization capable of providing services ranging from the definition of the problem to the actual design, testing, verification, and finally the implementation of solutions or measures. The Centre is currently the hub for Engineering, Research and Development that involved Canadian Universities, Government Laboratories, Canadian automotive parts and equipment suppliers. The Centre includes16 research and development test cells, prototype machine shop, PHEV, HEV and BEV development testing which occupies an area of 200,000 sq ft. The Centre is the hub for Production / Design Validation of engines manufactured in North America and an overflow for the Ford worldwide facilities. It also establishes a close link worldwide within Ford Research and Innovation Centre, Product Development and Manufacturing Operations that can help bridge the gap between laboratory research and the successful commercialization and integration of promising new technologies into the product development cycle.

His principal field of Research and Development encompasses the following: Optimizing Automotive Test systems for cost, performance and full compatibility. It includes the development of test methodology and cognitive systems; Calibration for internal combustion engines; Alternate fuels, bio fuels, lubricants and exhaust fluids; Lightweight materials with the focus on Aluminum, Magnesium, bio materials; Battery, Electric motors, super capacitors, stop/start systems, HEV, PHEV, BEV systems; Nano sensors and actuators; High performance and racing engines; Non-destructive monitoring of manufacturing and assembly processes; and Advanced gasoline and diesel engines focusing in fuel economy, performance and cost opportunities.

He has published and presented numerous technical papers in the above fields internationally. Dr. Tjong is also an Adjunct Professor of the University of Windsor, McMaster University, and University of Toronto. He continuously mentors graduate students in completing the course requirements as well as career development coaching.

Dr. Saeid Habibi is currently the Director of the Centre for Mechatronics and Hybrid Technology and a Professor in the Department of Mechanical Engineering at McMaster University. Saeid obtained his Ph.D. in Control Engineering from the University of Cambridge, U.K. His academic background includes research into intelligent control, state and parameter estimation, fault diagnosis and prediction, variable structure systems, and fluid power. The application areas for his research have included aerospace, automotive, water distribution, robotics, and actuation systems. He spent a number of years in industry as a Project Manager and Senior Consultant for Cambridge Control Ltd, U.K., and as Senior Manager of Systems Engineering for AlliedSignal Aerospace Canada. He received two corporate awards for his contributions to the AlliedSignal Systems Engineering Process in 1996 and 1997. He was the recipient of the Institution of Electrical Engineers (IEE) F.C. Williams best paper award in 1992 for his contribution to variable structure systems theory. He was also awarded an NSERC Canada International Postdoctoral Fellowship that he held at the University of Toronto from 1993 to 1995, and more recently a Boeing Visiting Scholar sponsorship for 2005. Saeid is on the Editorial Board of the Transactions of the Canadian Society of Mechanical Engineers and is a member of IEEE, ASME, and the ASME Fluid Power Systems Division Executive Committee.